



The switching mechanism of the bacterial rotary motor combines tight regulation with inherent flexibility

Oshri Afanar^{1,†} , Diana Di Paolo², Miriam Eisenstein³, Kohava Levi¹, Anne Plochowietz^{2,‡}, Achillefs N Kapanidis², Richard Michael Berry² & Michael Eisenbach^{1,*} 

Abstract

Regulatory switches are wide spread in many biological systems. Uniquely among them, the switch of the bacterial flagellar motor is not an on/off switch but rather controls the motor's direction of rotation in response to binding of the signaling protein CheY. Despite its extensive study, the molecular mechanism underlying this switch has remained largely unclear. Here, we resolved the functions of each of the three CheY-binding sites at the switch in *E. coli*, as well as their different dependencies on phosphorylation and acetylation of CheY. Based on this, we propose that CheY motor switching activity is potentiated upon binding to the first site. Binding of potentiated CheY to the second site produces unstable switching and at the same time enables CheY binding to the third site, an event that stabilizes the switched state. Thereby, this mechanism exemplifies a unique combination of tight motor regulation with inherent switching flexibility.

Keywords acetylated CheY; bacterial chemotaxis; bacterial flagellar motor; flagellar switch; molecular switch

Subject Category Microbiology, Virology & Host Pathogen Interaction

DOI 10.15252/emboj.2020104683 | Received 12 February 2020 | Revised 17 December 2020 | Accepted 19 January 2021 | Published online 23 February 2021
The EMBO Journal (2021) 40: e104683

Introduction

Switches are vastly known throughout the field of biology, from transcription and expression of genes to controlling processes of signal transduction, cell fate and cell cycle, to mention a few (Cross *et al*, 2002; Laslo *et al*, 2006; Pomerening, 2008). Most of these switches turn processes on and off. An exception is the switch of the bacterial flagellar motor, which controls the motor's direction of rotation rather than an on/off process (Eisenbach & Caplan, 1998). This dissimilarity

combined with this switch's unique properties—controlling a mechanical rather than a chemical process and being exceptionally ultrasensitive with respect to the switching signal (see below) (Cluzel *et al*, 2000), made it a challenging system of investigation. Indeed, in spite of decades of studies, the molecular mechanism underlying switching of the bacterial flagellar motor has remained obscure.

Switching of the motor enables bacterial cells to navigate. In bacteria like *Escherichia coli*, each cell contains multiple flagellar motors. When they rotate counterclockwise, the cell swims in a rather straight line, termed a “run”. When a considerable fraction of flagella switch from the default direction of rotation, counterclockwise, to clockwise, the cell preforms a chaotic-like turning motion, termed a “tumble” (Berg & Brown, 1972; Turner *et al*, 2000) (Fig 1 A), as a result of which the subsequent run (when the rotation switches back to counterclockwise) is in a randomly new direction. Conversely, very brief switching of some of the motors to clockwise generates slight changes in swimming direction without randomization rather than tumbles (Turner *et al*, 2000), thus maintaining directional swimming persistence (Vladimirov *et al*, 2010; Saragosti *et al*, 2011). This behavior was proposed to markedly improve the performance of collective migration (Saragosti *et al*, 2011), implying an evolutionary advantage. Maintenance of directional persistence requires extremely short intervals of clockwise rotation. However, it is unclear how the motor is regulated to produce both long clockwise intervals for tumbling and short intervals for directional persistence.

While the mechanism of switching is not resolved, much is known about the components of the switching machinery and the interactions between them. The switch of the flagellar motor is a large complex at the motor's base, consisting of multiple copies of the proteins FlhM, FlhN, and FlhG (Fig 1A). Since chemotaxis of bacteria is achieved by modulating the direction of flagellar rotation, the main control target in chemotaxis is the switch. The switch shifts the direction of rotation from counterclockwise to clockwise in response to binding the signaling protein CheY, which shuttles back and forth between the chemotaxis receptor complex and the

¹ Department of Biomolecular Sciences, The Weizmann Institute of Science, Rehovot, Israel

² Biological Physics Research Group, Clarendon Laboratory, Department of Physics, University of Oxford, Oxford, UK

³ Department of Chemical Research Support, The Weizmann Institute of Science, Rehovot, Israel

*Corresponding author. Tel: +972 8 9343923; E-mail: m.eisenbach@weizmann.ac.il

†Present address: Department of Chemical and Systems Biology, Stanford University, Stanford, CA, USA

‡Present address: Hardware Research and Technology Laboratory, Palo Alto Research Center, Palo Alto, CA, USA

flagellar switch. Earlier studies of the corresponding author's group revealed that phosphorylated CheY (CheY~P) mainly binds to the switch at the N terminus of FliM (FliM_N) (Welch *et al.*, 1993; Bren & Eisenbach, 1998). Subsequently, Blair's group reported on two additional sites with weaker binding of CheY (termed hereafter "low-affinity sites"), one at FliN, to which the binding is FliM_N-dependent and requires that CheY would be phosphorylated (Sarkar *et al.*, 2010), and one at FliM at other location than FliM_N (Mathews *et al.*, 1998). On the basis of this evidence combined with mutational analysis and a structural model, this group further suggested that the interaction of CheY~P with FliM_N serves to capture CheY~P and that switching to clockwise rotation involves the subsequent interaction of CheY~P with FliN (Sarkar *et al.*, 2010). NMR analysis in *Thermotoga maritima* by Dahlquist's group identified the middle domain of

FliM (FliM_M) as a low-affinity binding site for CheY (Dyer *et al.*, 2009). In view of this information, it is reasonable to assume that, also in *E. coli*, the other binding site is FliM_M. (For simplicity, we will term hereafter this other site in *E. coli* FliM_M even though its exact location is obscure.) It is not yet known how CheY binding to each of these sites affects the process of clockwise generation.

CheY is bound to receptor clusters at the cell's poles. It is well established that it has to be activated by phosphorylation for switching the motor to clockwise. This activation results in CheY~P dissociation from the poles and, as mentioned above, in binding to FliM_N. The level of CheY phosphorylation is regulated by CheA and CheZ as specific kinase and phosphatase, respectively (Fig 1A). A receptor-mediated attractant response (or removal of a repellent) inhibits CheA activity; stimulation by repellents (or attractant removal)

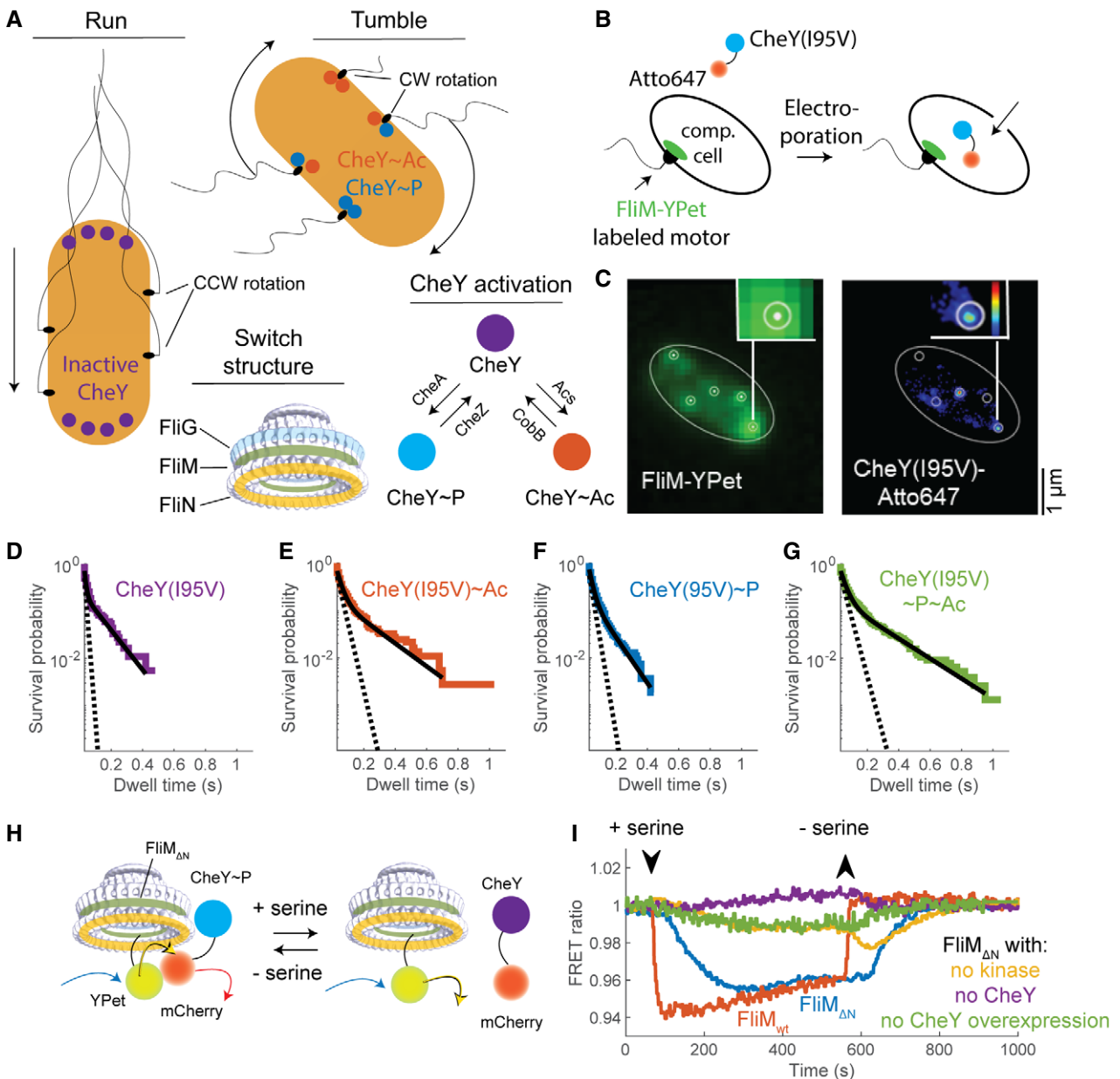


Figure 1.

Figure 1. Two modes of CheY binding to the switch.

- A Run-and-tumble swimming modes in *E. coli* are regulated by CheY activation by phosphorylation or acetylation. The electron density map of the switch was produced by Thomas *et al* (2006) and downloaded from <http://dx.doi.org/10.1093/nar/gkv1126>.
- B Scheme demonstrating the internalization of Atto647-labeled CheY(195V) to single cells by electroporation.
- C Demonstration of single-molecule tracking in a single cell. Cell outline is shown as an ellipse. Left, Imaged FliM-YPet fluorescence. White dots indicate the estimated motor locations. White circles illustrate a 75 nm radius around these locations. Right, Contour map of the normalized sum of probabilities of the localization events of CheY(195V)-Atto647 (from blue to red is low to high; black is zero probability). White circles show the motors' locations from the left panel.
- D Survival probabilities of unmodified CheY(195V)-Atto647 at the switch ($\Delta cheA$ background; strain EW668). 63 cells were recorded with a total of 1,316 trajectories in which CheY was found to interact with FliM. Note the logarithmic scale of the ordinate. Black line, a bi-exponential fit; dashed line, a fit of the fast decline process (see text for details).
- E As in (D) for acetylated CheY(195V)-Atto647 (presence of acetate, 50 mM, pH 7.0; strain EW668). 56 cells were recorded with a total of 1,904 trajectories.
- F As in (D) for phosphorylated CheY(195V)-Atto647 ($\Delta cheZ$ background; strain EW669). 82 cells were recorded with a total of 2,414 trajectories.
- G As in (D) for phosphorylated and acetylated CheY(195V)-Atto647 (presence of acetate, 50 mM, pH 7.0; $\Delta cheZ$ background, strain EW669). 40 cells were recorded with a total of 2660 trajectories.
- H Experimental scheme of the FRET experiment. The attractant serine lowers the phosphorylation level of CheY. As a result, CheY dissociates from the switch and the energy transfer from YPet (conjugated to FliM) to mCherry (conjugated to CheY) is reduced.
- I CheY interacts with FliM_{AN} and this interaction is sensitive to chemotactic stimuli. Each curve is the mean of two FRET measurements of cells in response to an attractant stimulus (0.1 mM serine; in the case of FliM_{wt}, a single measurement was performed with serine; another measurement of FliM_{wt} with 1mM aspartate produced similar results). See Appendix Fig S1 for the details of FRET analysis. FRET ratio is the ratio of mCherry to YPet fluorescence. CheY-mCherry and mCherry concentrations were $\sim 170 \mu\text{M}$ in the case of FliM_{AN} and $\sim 15 \mu\text{M}$ in the case of FliM_{wt} (Appendix Fig S2 for calibration of CheY concentration). Strains used: EW677 (FliM_{wt}, red), EW659 (negative control of FliM_{AN} without CheY, purple), EW637 (FliM_{AN}, blue), and EW636 (FliM_{AN} $\Delta cheA$, yellow).

enhances its activity [for reviews—(Berg, 2003; Eisenbach, 2004; Terashima *et al*, 2008; Porter *et al*, 2011)]. Another covalent modification that activates CheY to generate clockwise rotation is lysine acetylation (Wolfe *et al*, 1988; Barak *et al*, 1992, 1998). The regulation of acetylation is known to involve Acs and CobB as acetyl-transferase and deacetylase, respectively (Fig 1A) (Barak *et al*, 2004; Li *et al*, 2010). It has been shown that CheY acetylation is involved in bacterial chemotaxis (Barak & Eisenbach, 2001) and that it is inversely affected by CheA and CheZ (Barak & Eisenbach, 2004). Yet, the role that acetylated CheY (CheY~Ac) plays in chemotaxis is still obscure.

While the dependence of clockwise generation on the intracellular concentration of active CheY is highly cooperative, meaning that the motor is ultrasensitive (Cluzel *et al*, 2000), binding assays between CheY and the switch, carried out both *in vivo* and *in vitro*, found that the binding is non-cooperative (Sourjik & Berg, 2002; Sagi *et al*, 2003). Subsequent studies, which employed a constitutively active CheY mutant protein, found that it binds better to clockwise-rotating motors than to counterclockwise-rotating motors (Fukuoka *et al*, 2014). This difference in binding may well result in cooperativity of binding (Duke *et al*, 2001).

Here, we addressed the question of the mechanism underlying the switch function. We demonstrate that delicate, hitherto unknown, steps of the switching mechanism are resolved when FliM_N is truncated from the switch. We bring evidence for three sequential steps of CheY binding to distinct sites at the switch, each with a different outcome. Binding to the first site (FliM_N) potentiates CheY at the switch. Binding of potentiated CheY to the second site (FliN) is short-lived and generates transient motor switching. This seems to enable firm CheY binding to the third site (FliM_M), with a resultant stabilization of the switched state.

Results

Two dwelling modes of CheY at the switch; phosphorylation affects one mode, acetylation affects both

Following the findings of Fukuoka *et al* (2014), mentioned just above, that constitutively active CheY binds differently to

counterclockwise- and clockwise-rotating motors, we investigated whether two modes of binding can also be observed with CheY activated by phosphorylation and acetylation. To this end, we measured *in vivo* the dwell time of single CheY molecules at motors whose FliM molecules were labeled with YPet. We compared between phosphorylating conditions, acetylating conditions, and conditions under which CheY was both phosphorylated and acetylated. We electroporated CheY(195V) molecules labeled with a maleimide modification of the photo-stable organic dye Atto647 into FliM-YPet expressing cells (Fig 1B) (Di Paolo *et al*, 2016). The experiments were carried out in the following settings: in a $\Delta cheZ$ background to make CheY fully phosphorylated, in a $\Delta cheA$ background to make CheY non-phosphorylated, and, in each of these settings, also in the presence of the acetyl donor acetate to make CheY acetylated (Barak *et al*, 1992, 2004). The *cheY*(195V) mutation was designed to increase CheY affinity for FliM_N (Schuster *et al*, 2000), thus enhancing sampling of otherwise rare binding events. Custom-written software tracked CheY(195V)-Atto647 molecules and estimated switch locations in each cell using FliM-YPet fluorescence images. We interpreted CheY(195V)-Atto647 molecules dwelling within 75 nm of a switch for >30 ms as binding to the motor (Fig 1C; see Materials and Methods). We observed CheY(195V)-Atto647 molecules dwelling at the motor both in the absence and presence of acetate. However, in the latter case, the dwell time was markedly longer (Fig 1D vs. E and Fig 1F vs. G for the survival probability, i.e., for the probability to remain bound to the switch; Movie EV1). Notably, the very long dwell events in Movie EV1 were only detected in the presence of acetate.

The survival distributions in all experiments appeared to be biphasic, i.e., each of them comprised two exponentially decaying distributions, fast and slow (note the logarithmic scale of the ordinates in Fig 1D–G). A biphasic distribution is indicative of two modes of CheY dissociation from the switch, fast and slow. These two modes can either reflect CheY binding to two different sites at the switch or to two different states of the same site.

To quantify the effect of phosphorylation and acetylation on each mode, we fitted each of the distributions in Fig 1D–G with a bi-exponential expression $[A_1 e^{(-k_1 t)} + A_2 e^{(-k_2 t)}]$, with pre-exponential factors

$A_1 > A_2$, marking the fraction of each mode in the overall distribution, and k_1, k_2 being the rate constants of the modes; t is time]. From the fitted rate constants (and their inverse, the average dwell time of CheY at the switch), we could learn how phosphorylation, acetylation, or both modifications combined, affected each mode of CheY binding. Unmodified CheY exhibited the fastest decline rate in both modes (k_1 and k_2 being 99.5 and 9.7 s^{-1} , and expected average dwell times being about 10 and 100 ms, respectively; Fig 1D). Phosphorylation markedly decreased the rate of the fast mode, but did not affect the slow mode (k_1 and k_2 being 45.3 and 11.1 s^{-1} , and expected average dwell times being about 22 and 90 ms, respectively; Fig 1F). Acetylation alone decreased the decline rate of both modes (k_1 and k_2 being 32.8 and 5.6 s^{-1} , and typical dwell times being about 30 and 180 ms, respectively; Fig 1E). Phosphorylation and acetylation combined yielded values comparable to acetylation alone (k_1 and k_2 being 28.7 and 4.9 s^{-1} , and typical dwell times being about 35 and 200 ms, respectively; Fig 1G). Hence, it seems that phosphorylation mostly affects the fast mode, i.e., the mode with relatively short dwell times at the motor, whereas acetylation likely affects both modes.

CheY binds to the switch even in the absence of FliM_N

To study the association of both binding modes with clockwise generation, we sought to read the direct output of these modes. We suspected that the high-affinity binding of CheY to FliM_N might mask fine outputs related to these binding modes. Therefore, we studied the binding and functional interaction of CheY with motors in which FliM had been truncated to remove FliM_N (termed hereafter FliM_{ΔN}), i.e., with motors that only contained the low-affinity binding sites of CheY. To examine whether CheY can at all bind to such motors, we employed *in vivo* Förster resonance energy transfer (FRET), measuring the interaction between overexpressed CheY-mCherry and FliM_{ΔN}-YPet-labeled motors (Fig 1H for an explanatory scheme). First, to validate our FRET approach, we measured the response of non-truncated FliM (termed hereafter FliM_{wt})-YPet motors in cells that expressed CheY-mCherry to approximately the endogenous CheY expression level (due to leaky promoter expression; no inducer added). With these cells, the addition and subsequent removal of the attractant serine caused reduction and enhancement of the FRET signal, respectively, thus validating the method (Fig 1I, red curve). To determine whether CheY binds to FliM_{ΔN} (within the switch or soluble in the cytoplasm), we repeated the experiment with FliM_{ΔN}-YPet in cells expressing CheY-mCherry, using $\Delta cheZ$ background to ensure that CheY-mCherry was mostly phosphorylated. We observed a very weak, hardly detectable FRET response when the intracellular CheY-mCherry concentration was comparable to the endogenous CheY expression level (Fig 1I, green). However, when we overexpressed CheY-mCherry (inducer present), we observed a response similar in amplitude to that of FliM_{wt} (Fig 1I, blue). This difference between cells containing FliM_{wt} motors and cells containing FliM_{ΔN} motors was expected due to the absence of the high-affinity binding site from FliM_{ΔN} motors. These results imply a low-affinity interaction of CheY~P with FliM_{ΔN}. When, as a negative control, we overexpressed mCherry instead of CheY-mCherry, we observed no response (Fig 1I, purple). This implies that the FRET responses, observed with CheY-mCherry, did not emerge from an interaction between the fluorescent proteins

themselves. The response of FliM_{ΔN} cells overexpressing CheY-mCherry~P was slower than that of FliM_{wt} cells (Fig 1I). This was likely because of the longer time required to phosphorylate and dephosphorylate such high CheY concentrations and because of the possible impairment of the on-rate of CheY~P binding to the switch by the absence of FliM_N. The response of CheY-mCherry under conditions that do not allow its phosphorylation ($\Delta cheA$ background, i.e., the kinase is missing and the phosphatase is present) was minor (Fig 1I, yellow). This response possibly reflected the alternative pathway for chemotaxis, demonstrated in *E. coli* cells lacking most of the chemotaxis machinery but overexpressing CheY (Barak & Eisenbach, 1999).

To distinguish between CheY-mCherry binding to the switch and binding to free FliM_{ΔN}-YPet molecules within the cytoplasm, we attempted to measure CheY binding to individual motors, employing FRET photobleaching (Appendix Fig S3A and B). As detailed in Appendix 1, we indeed found an increased CheY~P binding at FliM_{ΔN}-YPet spots (presumably spots of individual motors) when the CheY-mCherry expression level was elevated (Appendix Fig S3C). However, as the CheY-mCherry concentration increased, the fluorescence of the spots became diffusive. This avoided conclusive differentiation between switch-originated and cytoplasm-originated signals (Appendix 1).

To verify that CheY~P can, indeed, bind to FliM_{ΔN} motors, we examined whether it can generate clockwise rotation of such motors, relying on the fact that, for generating clockwise rotation, CheY~P must first bind to the motor. We tethered cells containing FliM_{ΔN} motors (FliM_{ΔN}-YPet motors in some of the experiments) and ~100 μM CheY in a $\Delta cheZ$ background (to ensure phosphorylation of CheY) to glass via their flagella (Fig 2A for experimental scheme and Fig 2B for a demonstration of a tethered cell and for a representative trace of the rotation rate) and analyzed their direction of rotation with an automated home-made software. The mere overexpression of CheY was enough to produce clockwise rotation (Fig 2C prior to stimulation), indicating that CheY can bind to FliM_{ΔN} motors to generate clockwise rotation. The cells responded to positive stimuli (attractant addition or repellent removal) with reduced clockwise rotation (Fig 2C). Because positive stimuli work by lowering the phosphorylation level of CheY (Borkovich *et al*, 1989), the observed response implies that CheY had to be phosphorylated for binding to these FliM_{ΔN} motors. It also suggests that, as in cells containing FliM_{wt} motors (Sourjik & Berg, 2002), lowering the level of CheY~P results in lowering the clockwise level. Repellent stimulation, known to work by elevating the phosphorylation level of CheY (Sourjik & Berg, 2002), had hardly any effect (Fig 2D). This is because the absence of CheZ caused CheY to be fully phosphorylated already prior to the repellent stimulation. Thus, CheY~P functionally binds to FliM_{ΔN} motors.

FliM_{ΔN} motors respond differently to CheY~P and CheY~Ac

The observed different effects of phosphorylation and acetylation on the modes of CheY binding to FliM_{wt} motors (Fig 1D–G) raised the possibility that CheY~P and CheY~Ac generate clockwise rotation by somewhat different mechanisms. To examine this possibility, we compared clockwise generation by CheY, CheY~P, CheY~Ac, and CheY~P~Ac in cells containing FliM_{ΔN} motors. Studying FliM_{ΔN} motors is advantageous in this case because it avoids complications

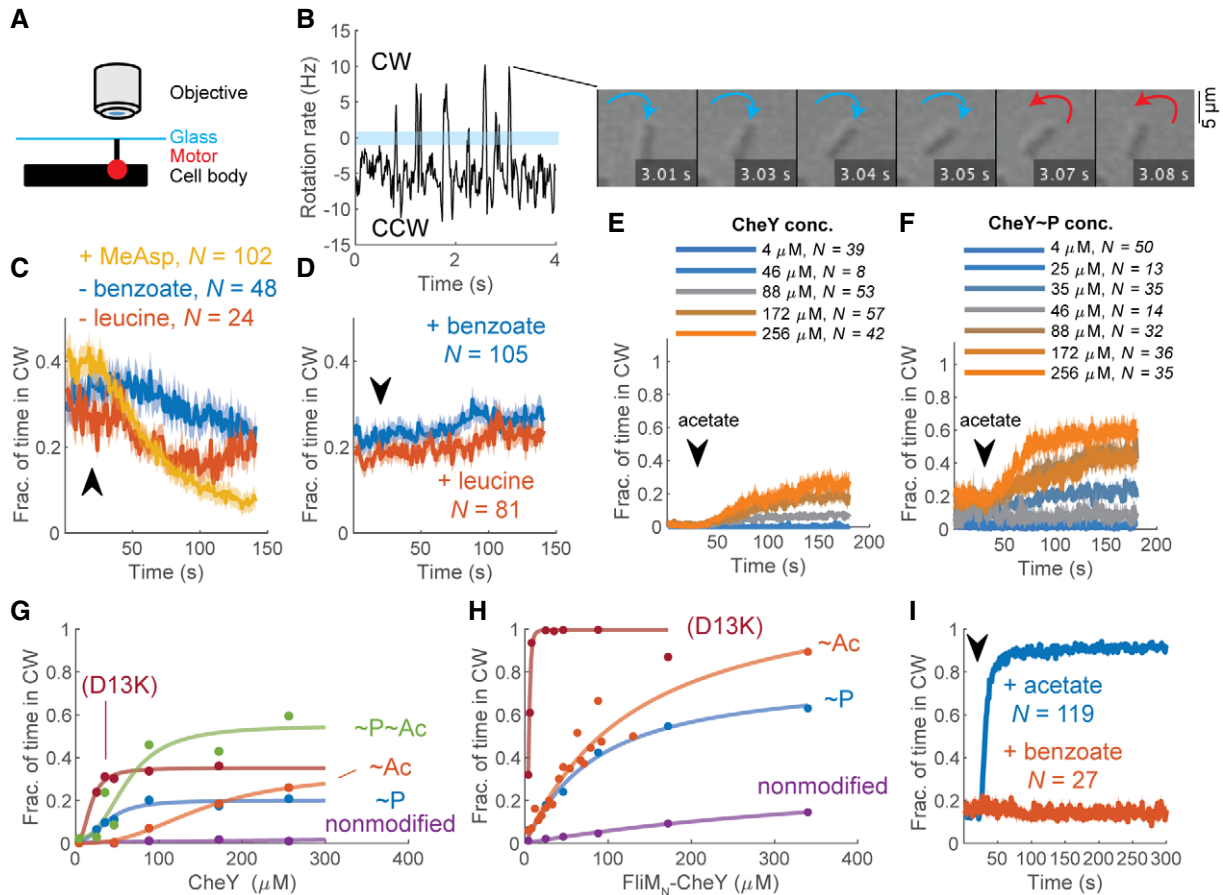


Figure 2. FliM_{ΔN} motors respond differently to various modifications of CheY and FliM_N-CheY.

- A Experimental scheme of flagellar motor tethering. The stub of sheared flagellum is tethered to glass by an anti-flagellin antibody (Silverman & Simon, 1974) in a flow chamber (Berg & Block, 1984).
- B Demonstration of rotation rate measured from a single cell; negative and positive values (below and above the blue bar) are counterclockwise and clockwise, respectively. The switch from negative to positive rotation rate at 3 s is shown in the montage to the right.
- C The response of tethered *fliM_{ΔN} ΔcheZ* cells (strain EW635), induced for CheY expression from a plasmid (200 μM IPTG), to positive stimuli. Lines and shaded regions are the mean time spent in clockwise rotation ± SEM. The arrow marks the estimated time at which the stimulant arrived to, or left (as indicated), the flow chamber. N is the number of cells. α-Methyl-DL-aspartate (MeAsp) and leucine were used at 1 mM, benzoate (pH 7.0) at 50 mM.
- D As in (C) for negative stimuli.
- E Response of tethered *fliM_{ΔN} ΔcheA* cells (strain EW634) to acetate (50 mM, pH 7.0) at different CheY concentrations. Lines and shaded regions are mean ± SEM.
- F Response of tethered *fliM_{ΔN} ΔcheZ* cells (strain EW635) to acetate. Details as in (E).
- G Contribution of acetylation and phosphorylation of CheY as well as its D13K mutation to clockwise rotation. The points are the mean clockwise rotation calculated from panels E and F at time segments 0–20 s and 160–180 s. The variants shown are *fliM_{ΔN} ΔcheZ* cells expressing CheY in the absence and presence of acetate (10 mM, pH 7.0) (i.e., CheY~P and CheY~P~Ac; blue and green curves; strain EW635), *fliM_{ΔN} ΔcheA* cells expressing CheY, in the absence and presence of acetate (CheY and CheY~Ac; purple and red, respectively; EW634), and *fliM_{ΔN} ΔcheA* cells expressing CheY(D13K) (burgundy; EW737). Each data point is the average of all experiments at a given CheY concentration, weighted by the sample number of each experiment. For data, see Table EV1. The CheY concentrations shown are estimates based on the calibration curves in Appendix Fig S2, for which a similar CheY expression system was used.
- H FliM_N further activates CheY variants to produce clockwise rotation. The variants shown are *fliM_{ΔN} ΔcheZ* cells expressing FliM_N-CheY (i.e., FliM_N-CheY~P; blue curve; strain EW697), *fliM_{ΔN} ΔcheA* cells expressing FliM_N-CheY, in the absence and presence of acetate (10 mM, pH 7.0) (FliM_N-CheY and FliM_N-CheY~Ac; purple and red, respectively; EW696), and *fliM_{ΔN} ΔcheA* cells expressing FliM_N-CheY(D13K) (burgundy; EW739). See G for other details.
- I Response of *fliM_{ΔN} ΔcheA* cells expressing FliM_N-CheY (strain EW696) to acetate and benzoate (10 mM each; pH 7.0). FliM_N-CheY expression was induced with 800 μM IPTG. Lines and shaded regions are the mean time spent in clockwise rotation ± SEM. The black arrow indicates the estimated time point at which the stimulus entered the flow chamber.

caused by differences in binding—CheY~P binds well to FliM_N (McEvoy *et al*, 1999) whereas CheY~Ac does not (Liarzi *et al*, 2010; Li *et al*, 2010). To assess the contribution of non-phosphorylated CheY to clockwise generation, we measured the clockwise level of cells that lacked the kinase of CheY (*ΔcheA* cells); for CheY~P, we

used cells that lacked the phosphatase of CheY (*ΔcheZ* cells); for CheY~Ac, we used *ΔcheA* cells supplied with the acetyl donor acetate (Appendix Fig S4 for a control of FliM_{ΔN} cells with intact chemotactic machinery, demonstrating that acetate acted as an acetyl donor rather than as a repellent); and for CheY~P~Ac, we

employed $\Delta cheZ$ cells supplied with acetate. To ascertain that the effects are not limited by CheY availability, we measured each of these CheY forms at increasing CheY concentrations that were far beyond the endogenous concentration of chromosomally expressed CheY [estimated at $\sim 10 \mu\text{M}$ (Li & Hazelbauer, 2004)]. While nonmodified CheY did not generate clockwise rotation (Fig 2E prior to acetate addition; Fig 2G, purple), CheY~P did (Fig 2F prior to acetate addition; Fig 2G, blue). Notably, the dependence of clockwise rotation on the CheY~P concentration had the shape of a saturation curve (Fig 2G, blue), unlike the ultrasensitive (sigmoidal, cooperative-like) dependence observed in FliM_{wt} motors (Cluzel *et al*, 2000). This suggests that the truncation of FliM_N resulted in loss of ultrasensitivity. Also, the concentration-dependence curve of clockwise rotation on CheY~P (Fig 2G, blue) further endorses the conclusion, made above, that the lack of a repellent response in Fig 2D was due to CheY being already fully phosphorylated rather than to a limiting CheY concentration.

The observation that CheY had to be activated by phosphorylation for generating clockwise rotation suggests that this clockwise response to CheY was due to specific interactions of CheY with the switch rather than to non-specific interactions within the switch, promoted by overexpressed CheY. To validate this conclusion and to confirm that the observed clockwise response was neither limited by CheY availability nor by its activation level, we employed CheY(D13K). The latter is a constitutively active mutant of CheY, which can be hardly phosphorylated (Bourret *et al*, 1990). CheY(D13K), too, generated clockwise rotation (Fig 2G, burgundy), endorsing the conclusion that the generation of clockwise rotation by CheY was due to its specific interaction with the switch. Moreover, CheY(D13K) performed better than CheY~P in generating clockwise rotation, implying that the D13K mutation activates CheY better than does phosphorylation. The reason for this higher activity is unclear as, to the best of our knowledge, the mechanism of CheY(D13K) activation is not yet resolved. Nevertheless, as in the case of CheY~P, clockwise generation by CheY(D13K) saturated at intermediate clockwise levels, confirming that clockwise generation was not limited by CheY availability. Thus, at this point we conclude that FliM_{ΔN} motors differ from FliM_{wt} motors in the sense that their response to CheY activated by phosphorylation or by D13K mutation is not ultrasensitive.

CheY~Ac also generated clockwise rotation (Fig 2E following acetate addition) but the dependence of clockwise generation on the CheY~Ac concentration was sigmoidal (cooperative-like), reaching saturation at high concentrations (Fig 2G, red). Clockwise generation by CheY~P~Ac (Fig 2F) was roughly the sum of the individual contributions of CheY~P and CheY~Ac to clockwise generation (Fig 2G, green). Thus, consistent with the finding that phosphorylation and acetylation bring about different effects on CheY binding to FliM_{wt} motors (Fig 1D–G), it seems that CheY~P and CheY~Ac differently generate clockwise rotation in FliM_{ΔN} motors (Fig 2G).

FliM_N fusion to CheY compensates for FliM_N truncation from the motor

The finding that FliM_N is not essential for CheY binding to the switch and for clockwise generation raised the question of what its role is. FliM_N promotes the interaction of CheY with the switch because, in its absence, CheY must be overexpressed for clockwise

generation [Fig 2G; the chromosomally expressed CheY concentration is $\sim 10 \mu\text{M}$ (Li & Hazelbauer, 2004)]. Therefore, a reasonable possibility, suggested earlier (Dyer *et al*, 2009; Sarkar *et al*, 2010), is that FliM_N tethers CheY to the switch, thereby elevating the local concentration of CheY at the low-affinity sites. According to this possibility, FliM_N acts as a “fishing line”, increasing the rate of CheY association with the clockwise-generating low-affinity sites at the switch. However, this might not be the only function of FliM_N. The observation that CheY, activated by phosphorylation, acetylation, or D13K mutation, saturated much before reaching maximal clockwise rotation (Fig 2G), suggests that activated CheY is insufficiently potent to produce full clockwise rotation in FliM_{ΔN} motors and that FliM_N is required for higher potency of CheY. It has been found that FliM_N-bound CheY adopts an intermediate conformation between the active and inactive states (Dyer & Dahlquist, 2006) and enhances the rate of CheY phosphorylation by small phosphodonors (Schuster *et al*, 2001). This begs the question of whether these observed features serve to increase CheY’s potency to generate clockwise rotation when it is tethered to FliM_N. To examine this possibility, we studied the motor’s behavior in a FliM_{ΔN} strain that expresses CheY fused to FliM_N (FliM_N-CheY) from a plasmid prepared and employed earlier by Sarkar *et al* (2010). We compared it with the motor’s behavior of the same strain that expresses wild-type CheY instead of FliM_N-CheY. The expression of both proteins was induced in parallel and under identical conditions to different levels by an IPTG-inducible promoter. We made this comparison in $\Delta cheZ$ and $\Delta cheA$ backgrounds, elevating and lowering CheY phosphorylation, respectively. In a $\Delta cheZ$ background, cells containing FliM_N-CheY~P spent much more time in clockwise rotation than cells containing CheY~P (compare blue curves in Fig 2H and G). The observation that the half-saturation concentrations (indicative of K_d) of these curves were similar, further suggests that the potentiation of CheY~P by FliM_N to generate more clockwise rotation is not due to stronger binding of FliM_N-CheY~P to the switch. Nevertheless, the saturation point of FliM_N-CheY~P was about threefold higher than that of CheY~P. It, thus, appears that when FliM_N is fused with CheY~P, the latter is more likely to be found in a conformation that is potent for clockwise generation. (We use here the term “potent” to distinguish from “active”, which denotes CheY activated by phosphorylation, acetylation, or mutation.) In a $\Delta cheA$ background, cells expressing FliM_N-CheY could generate low levels of clockwise rotation whereas cells expressing wild-type CheY could not produce clockwise rotation (purple curve in Fig 2H vs. G). This implies that CheY can acquire a potent clockwise-generating conformation as a result of binding to FliM_N.

To substantiate the conclusion that FliM_N potentiates CheY independently of phosphorylation, we studied the dose-dependent clockwise-generating activity of FliM_N-CheY(D13K) under non-phosphorylating conditions, i.e., in a $\Delta cheA$ background. The FliM_N fusion extremely increased the clockwise generation potency of CheY(D13K) (burgundy curve in Fig 2H vs. G), so much so that clockwise rotation could be generated just by the leaky expression of the protein from the plasmid (levels that were roughly equivalent to endogenous CheY expression levels). This effect at so low concentrations suggests that CheY(D13K) binding to the switch was specific. Thus, FliM_N fusion to CheY(D13K) substantially compensated for the FliM_N deletion from the switch. This strongly supports the notion that FliM_N functions to promote switching in a phosphorylation-independent manner.

Switching of FliM_{ΔN} motors involves two phases of distinct interval lengths

Acetylation, mediated by saturating concentrations of acetate, greatly enhanced clockwise rotation of FliM_N-CheY in FliM_{ΔN} motors (red curve in Fig 2H vs. G). This clockwise-generating effect of acetate was acetylation specific as benzoate, which acts as a repellent by the same mechanism as does acetate (Kihara & Macnab, 1981; Repaske & Adler, 1981) but does not serve as an acetyl donor (Barak *et al.*, 1992, 2004), had no effect on the clockwise rotation (Fig 2I). In batches in which we measured the dependence of clockwise rotation on FliM_N-CheY~Ac concentration at high resolution, we noticed that the dependence was biphasic, i.e., it comprised two consecutive saturation-like curves (Fig 3A). To the best of our knowledge, two phases of motor response to CheY have not been hitherto described.

When we measured, in the same strain, the motor's response to acetate removal (a decay process that only depends on FliM_N-CheY~Ac dissociation from the switch), we found that the decay was monophasic at low acetate concentrations and biphasic at high concentrations. Thus, at the two highest measured

acetate concentrations (5 and 10 mM), a slower response to acetate removal preceded the fast one (Fig 3B, dark- and bright-orange). When we fitted an exponential expression to the decay, we found that the fitted rate constants were similar at both concentrations (-0.095 and -0.006 s⁻¹ for the fast and slow phases at 5 mM acetate—Fig 3B, black straight lines, and -0.091 and -0.005 s⁻¹ for 10 mM acetate). However, only the fast phase was observed at lower concentrations (0.5 and 1 mM with fitted rate constants of -0.085 and -0.099 s⁻¹, respectively). Thus, in FliM_{ΔN} motors, both the dependence of clockwise generation on the concentration of intracellular FliM_N-CheY~Ac and the rate of the return to counterclockwise rotation appear to be biphasic.

A highly reasonable assumption is that switching of the motor is a random process, in which the life span of the clockwise state correlates with the lifetime of CheY binding to the motor. The apparent two phases, observed in Fig 3A, could potentially be a reflection of two concentration-dependent binding modes of FliM_N-CheY~Ac to the motor; one relatively weak binding and one relatively strong. If so, it might be expected that the life span of clockwise intervals would be distinct at low and high FliM_N-CheY~Ac concentrations.

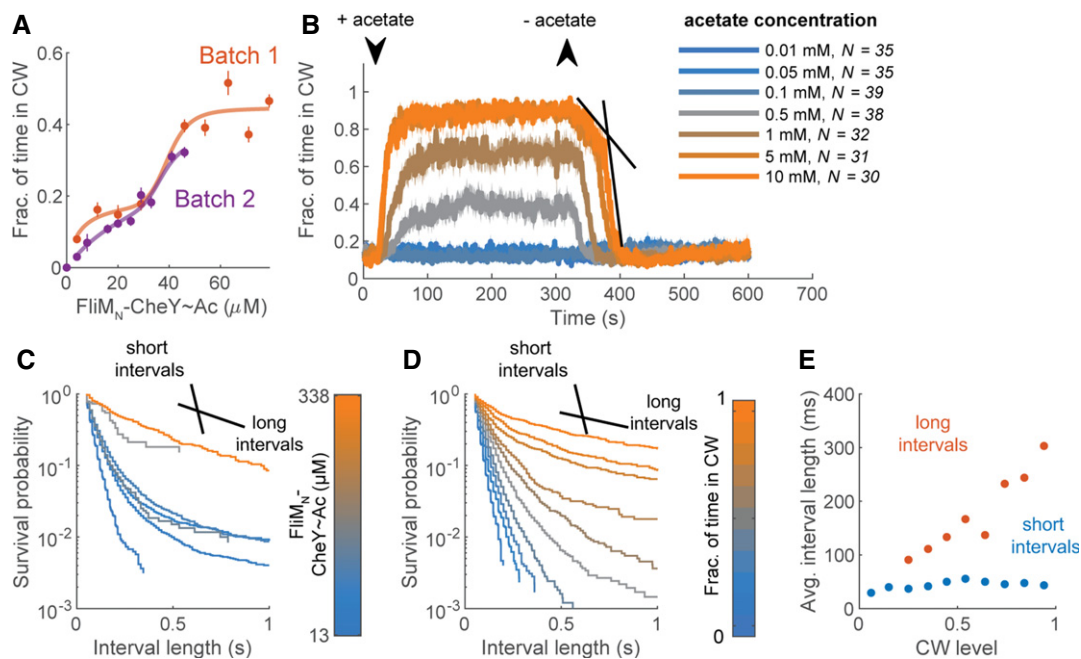


Figure 3. Biphasic switching of FliM_{ΔN} motors.

- A Dependence of clockwise rotation on the level of FliM_N-CheY~Ac. The red and purple curves are two experimental days in which the clockwise production by *fliM_{ΔN} ΔcheA* cells expressing FliM_N-CheY in the presence of acetate (10 mM, pH 7.0) was measured as a function of FliM_N-CheY concentration (strain EW696; these curves are partial data of the red curve in Fig 2H). Concentrations are estimates based on the calibration curves in Appendix Fig S2, for which a similar CheY expression system was used. Each data point is a mean ± SEM of the data shown in Table EV1 for the second and third experimental days of this strain (in the presence of acetate).
- B Response of the strain shown in (A) to addition and removal of varying acetate concentrations (pH 7.0). FliM_N-CheY concentration was estimated to be ~300 μM. Lines and shaded regions are the mean time spent in clockwise rotation ± SEM. The arrows indicate the estimated time points at which acetate entered or left the flow chamber. Black lines mark the linear part of the biphasic response to acetate removal. N is the number of cells.
- C Distribution of clockwise interval lengths at different FliM_N-CheY~Ac concentrations in the strain shown in (A). FliM_N-CheY was acetylated by acetate (10 mM, pH 7.0). The black lines illustrate the slopes of the short and long clockwise interval distributions. The color-bar indicates the estimated FliM_N-CheY~Ac concentration.
- D As in (C), but with distributions made with respect to the average clockwise levels of the cells.
- E Average clockwise interval length, calculated as the inverse of the fast (blue) and slow (red) rate constants from bi-exponential fits of the distributions in (D).

Such short and long clockwise life spans should be seen as fast and slow exponentially decaying distributions of clockwise intervals, respectively (as in Fig 1D–G; for simplicity, we will refer hereafter to these distributions by their average interval length, i.e., fast and slow decay will be referred to as short and long clockwise intervals, correspondingly). To determine whether indeed the two phases in Fig 3A are associated with different distributions of clockwise intervals, we measured and constructed distributions from the clockwise interval lengths produced by FliM_{AN} motors, as a function of FliM_N-CheY~Ac concentration (see Movie EV2 for a demonstration of rotation analysis). In Fig 3 C, we present the interval lengths in survival distributions. In first approximation, at the lowest and highest FliM_N-CheY~Ac concentrations we observed roughly single-exponential distributions, representing short and long clockwise intervals, respectively (Fig 3 C blue and orange; note the logarithmic scale of the ordinate, where exponential curves are straight lines). At intermediate FliM_N-CheY~Ac concentrations, the distribution of clockwise intervals was biphasic (i.e., a mixture of short and long clockwise intervals; Fig 3C, gray). These observations are consistent with the possibility that low and high FliM_N-CheY~Ac concentrations result in relatively weak and strong binding to the motor, respectively. Similar distributions of interval lengths were resolved when we clustered the interval lengths according to the average clockwise levels of the individual measured cells, which are likely a better proxy of CheY concentration at the switch (Fig 3D). To quantify the link between the phases of the clockwise intervals and the clockwise level, we fitted each of the distributions with a bi-exponential expression (as done for the single-molecule observations—Fig 1D–G), and plotted the average interval time of each phase, calculated from the fits, as a function of the average clockwise level of the cells (Fig 3E). We found that the fast-decaying part of the distribution produced short intervals, ~40 ms long, independently of the clockwise level (Fig 3E, blue). This interval length is at the same order of magnitude as the short dwell time of CheY~Ac at wild-type motors in the single-molecule experiment (30 ms; Fig 1E). As of clockwise level of ~0.25, the slowly decaying part of the distribution became apparent, and its clockwise intervals increased in length with the average clockwise level of the cells (Fig 3E, red). These intervals were relatively long, at the same order of magnitude as the long dwell time of CheY~Ac at wild-type motors in the single-molecule experiment (180 ms; Fig 1E). The different clockwise levels did not affect the rotation rate (Fig EV1A). The distribution of the counterclockwise intervals appeared to mirror the clockwise distributions (Fig EV1A). Similar results were obtained when CheY was activated by phosphorylation or by D13K substitution, with (Fig EV1B–E) or without (Fig EV2A) FliM_N fusion. This indicates that the mere appearance of short and long clockwise intervals is inherent to the switch's response to CheY. It is independent of how CheY was activated.

To summarize our observations thus far, we detected multiple signatures of two switching processes in FliM_{AN} motors. These include the dependence of clockwise generation on the level of FliM_N-CheY~Ac (Fig 3A), the time-dependent decrease in clockwise rotation upon CheY deacetylation (i.e., acetate removal; Fig 3B), and the sequential appearance of two types of clockwise interval lengths as a function of CheY levels (Fig 3C and D). Notably, a slow phase that precedes a fast phase (as in Fig 3B) may be

indicative of a sequential response. Indeed, a biphasic response that mimics the observed response could be generated in a mathematical model by assuming two dependent CheY-binding sites (Appendix Fig S5; see Discussion). Even though similar signatures of two switching processes were not noticed in earlier measurements (Scharf *et al*, 1998), probably due to the interfering effect of FliM_N, we think that the observation of two CheY dwelling phases at FliM_{wt} motors (Fig 1D–G) can be considered as such signatures in wild-type motors.

The existence of two CheY-binding sites other than FliM_N at the switch (Mathews *et al*, 1998; Dyer *et al*, 2009; Sarkar *et al*, 2010), along with the observed two phases of motor response to CheY (Fig 3), raised the question of whether these two phases are associated with the two different CheY-binding sites, FliN and FliM_M. To investigate this possibility, we examined whether a perturbation of any of these sites affects a distinct phase of clockwise generation.

Impaired CheY binding to FliN eliminates short clockwise intervals

We examined the involvement of FliN by studying the generation of clockwise rotation in a *fliN*(A93D) mutant, in which the interaction of FliM_N-CheY~P with FliN is greatly impaired (Sarkar *et al*, 2010). Clearly, this mutant was unable to generate clockwise rotation by FliM_N-CheY~P (Fig 4A, blue). This supports the conclusion of Sarkar *et al* (2010) that FliN is involved in FliM_N-CheY~P binding to produce switching. However, FliM_N-CheY~Ac and, the more so, FliM_N-CheY~Ac~P, led to significant clockwise rotation (Fig 4A, red and green, respectively).

The impairment of CheY interaction with FliN in the mutant was also reflected in motor's interval lengths. We calculated the distribution of the clockwise interval lengths of motors in this mutant under conditions like those in the experiment shown in Fig 3C and D ($\Delta cheA$ background in the presence of acetate). We found that the distribution of clockwise intervals slowly decayed (Fig 4B; Fig EV2B for additional parameters; Fig EV2C for cells containing FliM_N-CheY~Ac~P). The slope of the decay (Fig 4B) was similar to the decay slope of long clockwise intervals in FliN_{wt} motors (Fig 3 D). Excluding relatively rare events in cells with the highest measured clockwise level, none of the distributions could be fitted with a bi-exponential expression. A mono-exponential fit of the distributions resulted in average interval lengths similar to those observed for long intervals in FliN_{wt} motors (Fig 4C; cf. Fig 3E, red; in the case of the highest clockwise distributions, only the first, faster decaying distribution was included in the fit). This observation is consistent with the much lower reversal frequency of FliN(A93D) motors than that of FliN_{wt} motors (Fig EV2B and C vs. Fig EV1A and C, respectively). Thus, it appears that short clockwise intervals are relatively rare when CheY binding to FliN is impaired, suggesting that CheY binding to FliN generates short intervals of clockwise rotation. Since the dwell time of CheY at the switch is likely correlated with the length of the clockwise interval, this can also imply that CheY binding to FliN is short-lived.

Consistently, the FliN(A93D) motors responded to acetate removal in a monophasic decay of clockwise rotation (Fig 4D, red; the decay's rate constant was $0.0135 \pm 0.0027 \text{ s}^{-1}$, mean \pm SD of the three measurements), which was comparable in rate to that of

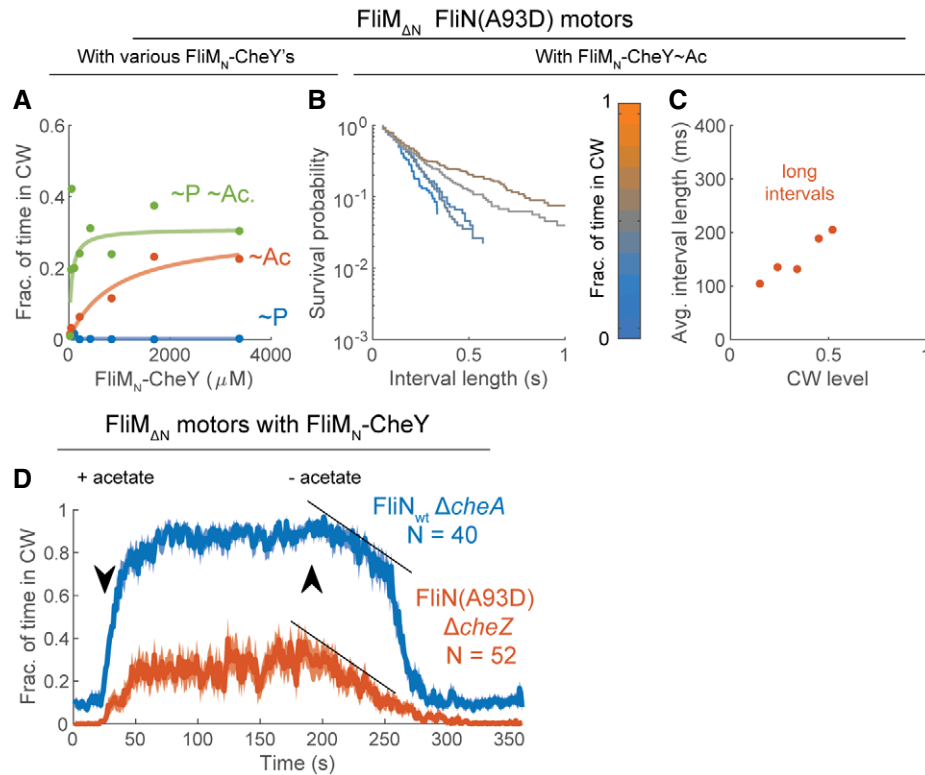


Figure 4. Impairment of FliM_N-CheY binding to FliN results in long clockwise intervals.

- A Effects of FliM_N-CheY acetylation and phosphorylation on clockwise rotation of tethered cells containing FliM_{ΔN} FliN(A93D) motors. Acetate concentration was 10 mM each (pH 7.0). FliM_N-CheY and FliM_N-CheY~P were produced by using ΔcheA and ΔcheZ backgrounds (strains EW713 and EW714), respectively. Each data point is the average of all measurements at a given FliM_N-CheY concentration, weighted by the sample number of each experiment. The concentrations shown are estimates based on the calibration curves in Appendix Fig S2, for which a similar CheY expression system was used. Concentrations larger than 500 μM were calculated by the linear extrapolation of the calibration curve. For data see Table EV1.
- B Distribution of clockwise interval lengths at different average clockwise levels in ΔcheA cells containing FliM_{ΔN} FliN(A93D) motors and expressing FliM_N-CheY (strain EW713), in the presence of acetate (10 mM, pH 7.0).
- C Average clockwise interval length, calculated as the inverse of the rate constants from monophasic fits of the distributions in (B).
- D Response of tethered ΔcheZ cells having FliM_{ΔN} FliN(A93D) motors to acetate addition and removal (red; strain EW714; FliM_N-CheY concentration estimated at ~300 μM). Similar results were obtained with a ΔcheA strain (EW713). Tethered cells having FliM_{ΔN} FliN_{wt} motors and containing FliM_N-CheY (strain EW696) are shown for reference (blue; this is the orange curve in Fig 3B after cutting some time segments before and after acetate removal to synchronize with the other response). Acetate concentration was 10 mM (pH 7.0). The data shown are the mean ± SEM. N is the number of cells. Black lines indicate the clockwise-decay rates of FliN_{wt} motors' slow phase and of FliN(A93D) motors following acetate removal.

the slow decay phase in FliM_{ΔN} FliN_{wt} motors (Fig 4D, blue). The suppression of short clockwise intervals (Fig 4B and C) and of the fast decay rate (Fig 4D) when CheY interaction with FliN was impaired are in-line with the proposition that CheY binding to FliN is short lived. They further suggest that long intervals are produced by CheY interaction with a switch site other than FliN.

Alteration of CheY binding to FliM_M affects long clockwise intervals

As mentioned above, an obvious candidate for this other switch site is FliM_M, shown to bind CheY in *T. maritima* (Dyer et al., 2009). To examine the plausibility of CheY binding to FliM_M in *E. coli*, we employed *in vivo* crosslinking of cells expressing FliM_{ΔN}-YPet, using a non-specific crosslinker, glutaraldehyde. The advantage of using crosslinking is that, beyond being carried out *in vivo*, it can detect weak interactions. (We wish to point out that FRET experiments

in vivo cannot distinguish between CheY binding to FliM and FliN due to being in close physical proximity to each other.) We tracked the crosslinking products by SDS-PAGE and scanning the gel for FliM_{ΔN}-YPet fluorescence. This enabled us to quantify the extent of complex formation. Among many other crosslinking products, we obtained a product at the size of a complex between FliM_{ΔN}-YPet and CheY (Fig 5A, lanes 1–3). When CheY was potentiated by FliM_N fusion, the complex formed with FliM_{ΔN} was shifted by about the molecular mass of FliM_N, and the amount of complex formation seemed higher (Fig 5A, lanes 4–6; the band of the shifted complex overlapped with an existing background band so the extent of excess complex formation due to CheY potentiation was hard to estimate). The formation of this complex was dependent on CheY over-expression (Appendix Fig S6), implying that the complex indeed contained CheY. These observations are consistent with the possibility of CheY binding to FliM_M *in vivo*, but they do not rule out a possibility of CheY binding to another FliM domain (e.g., to the C

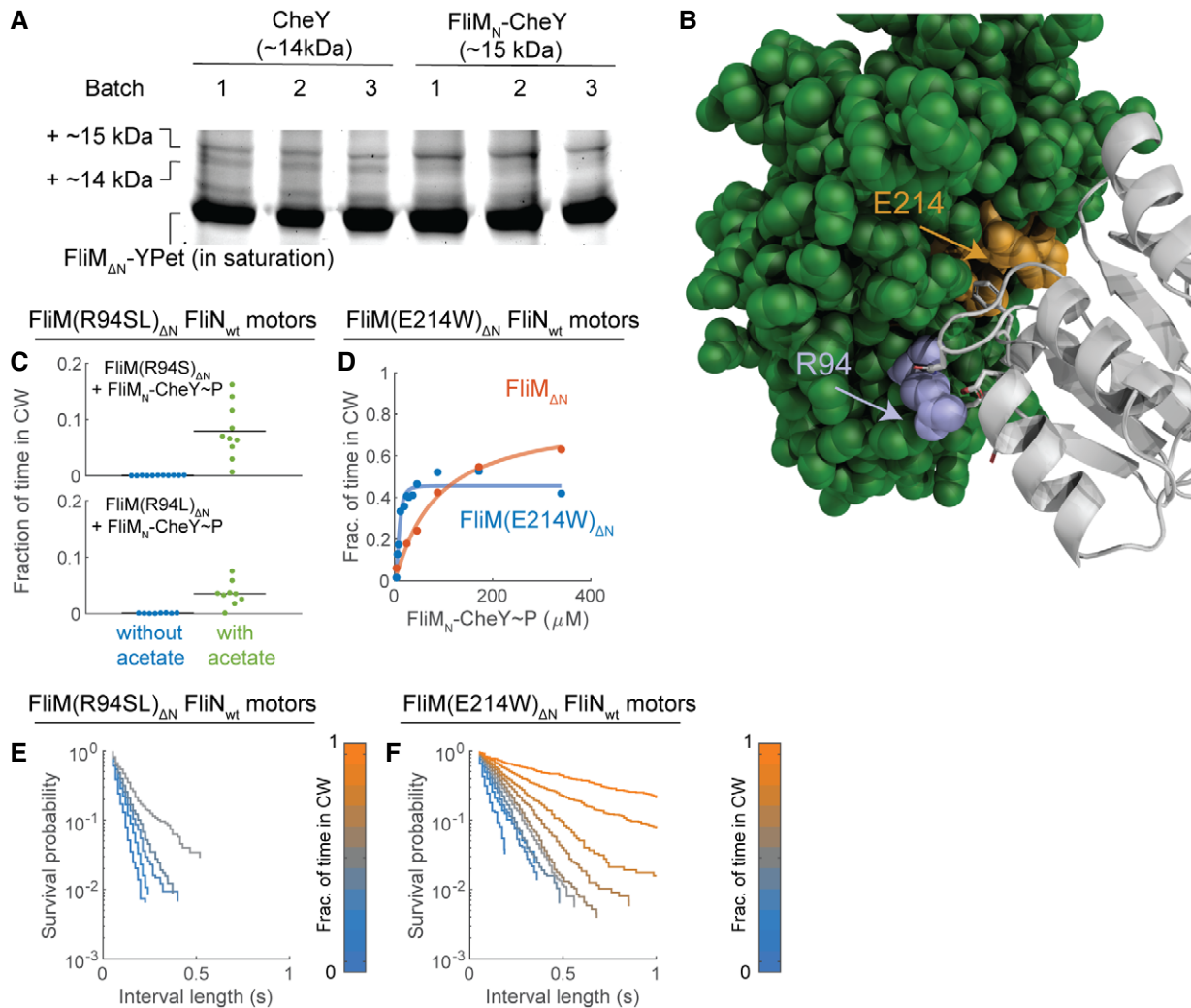


Figure 5. Mutations designed to impair and enhance CheY binding to FliM_M produce short and long clockwise intervals, respectively.

- A CheY crosslinks with FliM_{ΔN}-YPet *in vivo*. The cytoplasm of *fliM*_{ΔN}-YPet Δ*cheZ* cells overexpressing CheY (strain EW694) or FliM_N-CheY (strain EW697) from a plasmid was crosslinked by glutaraldehyde and resolved by SDS-PAGE. 1, 2, 3 stand for three different experiments that underwent this procedure. The plus sign before ~ 14 and ~ 15 stands for + 55 kDa of FliM_{ΔN}-YPet. Note that gel running suffered from parabolic distortion in band positions. The annotations relate to the lowest positions of the bands. The gel was imaged for FliM_{ΔN}-YPet fluorescence. To see the crosslinking products, the intense fluorescence of monomeric FliM_{ΔN}-YPet is shown at saturation. See Appendix Fig S6 for additional details.
- B Predicted binding interfaces of CheY (gray ribbon) and FliM_M (green spheres) in *E. coli*. R94 of FliM is shown in blue. Part of the hydrophobic region of FliM (including E214) is shown in orange.
- C Clockwise rotation of tethered *fliM*(R94S)_{ΔN} Δ*cheZ* cells and *fliM*(R94L)_{ΔN} Δ*cheZ* cells expressing FliM_N-CheY (strains EW731 and EW733, respectively) in the absence or presence of acetate (10 mM, pH 7.0). FliM_N-CheY concentration was estimated to be ~ 4 mM by extrapolation of the calibration curves in Appendix Fig S2, for which a similar CheY expression system was used. No clockwise rotation was observed when benzoate substituted for acetate. Each data point is the mean of a separate experiment. Black line is the mean of all experiments. For sample number of each data point see Table EV1.
- D Clockwise rotation of tethered *fliM*(E214W)_{ΔN} Δ*cheZ* cells (strain EW718) at various concentrations of FliM_N-CheY. The concentrations shown are estimates based on the calibration curve in Appendix Fig S2, for which a similar CheY expression system was used. Each data point is the average of all measurements at similar FliM_N-CheY concentrations, weighted by the sample number of each experiment. The red points and curve are taken, as a reference, from Fig 2H. For data see Table EV1.
- E Distribution of clockwise intervals of *fliM*(R94S)_{ΔN} Δ*cheZ* cells expressing FliM_N-CheY (strains EW732 and EW734) in the presence of acetate (10 mM, pH 7).
- F Distribution of clockwise intervals of *fliM*(E214W)_{ΔN} Δ*cheZ* cells expressing FliM_N-CheY (strain EW718) in the absence of acetate.

terminus domain of FliM). Various direct *in vitro* binding assays between purified CheY and FliM_{ΔN} were not conclusive, probably due to the low affinity of FliM_{ΔN} for CheY.

To examine the likelihood that CheY binding to FliM_M is functional, we employed docking analysis between CheY and FliM_M

based on their binding interface in *T. maritima* (Appendix Supplementary Methods for detailed description). In the docking analysis, we produced a number of models of CheY binding to FliM_M in *T. maritima* and translated those fitted well with the NMR results of Dyer *et al* (2009) to *E. coli* proteins by superposing the active and

inactive forms of CheY upon the model of FliM_M. We substantiated the superposition results by docking the *E. coli* proteins independently of the *T. maritima* model. The analysis predicted two prominent latching interfaces of CheY with FliM_M: an electrostatic interface, mostly contributed by arginine at position 94 of FliM, and a hydrophobic pocket in FliM, predicted to face the phosphorylation site of CheY (Fig 5B, blue and orange for electrostatic and hydrophobic surfaces, respectively).

To determine the relevance of the binding interface predictions, we studied motors with substituted arginine at position 94 (Appendix Fig S7A) as well as motors with substituted glutamic acid at position 214 (Appendix Fig S7B). The first substitution was designed to diminish electrostatic interactions, whereas the substitution at position 214 was designed to enhance hydrophobic interactions by replacing a charged residue with a bulky hydrophobic one. Thus, to determine the relevance of the predicted electrostatic interaction, we examined the rotation of motors of cells expressing FliM_{ΔN}(R94S) or FliM_{ΔN}(R94L) in a *ΔcheZ* background and overexpressing FliM_N-CheY (i.e., FliM_N-CheY~P). The motors of these mutants did not rotate clockwise (Fig 5C, blue). Only when acetate was present, i.e., when CheY was both phosphorylated and acetylated, we observed low levels of clockwise rotation (Fig 5C, green). These results are in-line with the docking model's prediction that FliM(R94) is involved in CheY binding. To determine the functional relevance of the predicted hydrophobic interaction, we could not just diminish this interaction by a simple mutation, as we did for the electrostatic interaction, because the hydrophobic area is contributed by many residues. Therefore, we examined, instead, whether enhancement of hydrophobic interactions by replacement of a charged residue with a hydrophobic one in the hydrophobic CheY-FliM_M-binding interface (E214W) would increase clockwise generation. Indeed, clockwise rotation in the *fliM*_{ΔN}(E214W) mutant in a *ΔcheZ* background was observed at much lower FliM_N-CheY expression levels (Fig 5D). It appears that the mutation affected the motor's sensitivity to CheY rather than affecting its intrinsic clockwise level. This is because the clockwise rotation levels of *fliM*_{ΔN}(E214W) in a *ΔcheA* background, where FliM_N-CheY is mostly inactive and does not contribute much to clockwise generation, were low and comparable to cells containing nonmutated FliM_{ΔN} (Appendix Fig S8; blue). Yet, when FliM_N-CheY was activated by acetate, the response of cells with FliM_{ΔN}(E214W) motors exceeded that of cells with nonmutated FliM_{ΔN} (Appendix Fig S8; red).

To examine our prediction that CheY interaction with FliM_M generates long clockwise intervals, i.e., stable clockwise rotation, we produced distributions of clockwise interval lengths in the *fliM*_{ΔN}(R94SL) and *fliM*_{ΔN}(E214W) mutants. Excluding cells with the highest measured clockwise level, *fliM*_{ΔN}(R94SL) motors yielded a single, exponentially decaying distribution of short clockwise intervals (Fig 5E; Fig EV2D for additional parameters). This is in-line with the expectation that attenuation of CheY interaction with FliM_M would diminish long clockwise intervals. The slope of the distribution was like the slope of the short intervals' phase in cells containing nonmutated FliM_{ΔN} motors (e.g., Fig 3D). Consistent with the anticipation that the elevation of CheY affinity for FliM_M would generate longer clockwise intervals, distributions produced by the *fliM*_{ΔN}(E214W) mutant were monophasic (Fig 5F; Fig EV2E for additional parameters). With the exception of

the lowest clockwise level, the slopes of the distributions were similar to those of the long intervals' phase in cells containing nonmutated FliM_{ΔN} motors (e.g., Fig 3D), meaning that short clockwise intervals were absent at most clockwise levels. Taken together, these results suggest that CheY binding to FliM_M produces long clockwise intervals.

Discussion

Of the many known biological switches, the switch of the bacterial flagellar motor has been a focus of great interest due to its unique properties. It has also been a source of frustration due to lack of success in resolving its molecular mechanism. In the current study, we revealed the functions of each of the three CheY-binding sites at the switch, FliM_N, FliM_M, and FliN. This led to uncovering processes at the switch that result in brief and long events of switching. Thus, we identified two modes of CheY binding to wild-type motors as well as to FliM_{ΔN} motors, and a number of related processes that essentially consist of two phases. These included the dependence of clockwise generation on the level of activated CheY (FliM_N-CheY~Ac), the time-dependent decrease in clockwise rotation upon CheY deactivation by acetate removal, and the motor's switching kinetics. Studying motors carrying mutations in FliN and FliM_M enabled us to detect the link between these sites and the biphasic processes, and to conclude that short clockwise intervals are mostly promoted by CheY binding to FliN, and long intervals—by CheY binding to FliM_M. The observations that the average durations of the short and long clockwise intervals of FliM_{ΔN} motors are similar to the short and long dwell time of CheY at wild-type motors, respectively, suggest that the conclusions drawn may be relevant to both FliM_{ΔN} motors and wild-type motors. The finding that CheY has to be acetylated for producing long clockwise intervals in motors defective in CheY-FliN binding further indicated that CheY~Ac is more effective than CheY~P in binding to FliM_M. Below we discuss implications of these findings and we show how they are related to each other in a model of the switching mechanism.

Functions of FliM_N

We found that the first site to which CheY binds, a high-affinity site at FliM_N (Welch *et al*, 1993; Bren & Eisenbach, 1998), is not essential for binding to the switch and for clockwise generation (Figs 1 and 2). Yet, the order-of-magnitude higher CheY concentration needed for binding and response in the absence of FliM_N (Figs 1 and 2) indicated that FliM_N is required for maximal sensitivity of the switch. FliM_N may do it by tethering CheY to the switch, but it seems that its most pronounced effect is to potentiate CheY (Fig 2H). To the best of our knowledge, this is the first system in which a ligand (CheY) is potentiated by its receptor (FliM at the switch), rather than *vice versa*.

The conclusion that FliM_N potentiates CheY is based on our studies with FliM_N-CheY fusion protein (Fig 2H). The published observation that CheY binds to FliM_N [$K_d = 27$ and $680 \mu\text{M}$ for CheY~P and CheY, respectively (McEvoy *et al*, 1999)] strongly suggests that this potentiation also occurs *in vivo* with non-fused proteins. CheY potentiation at the switch may be a preliminary step in the process

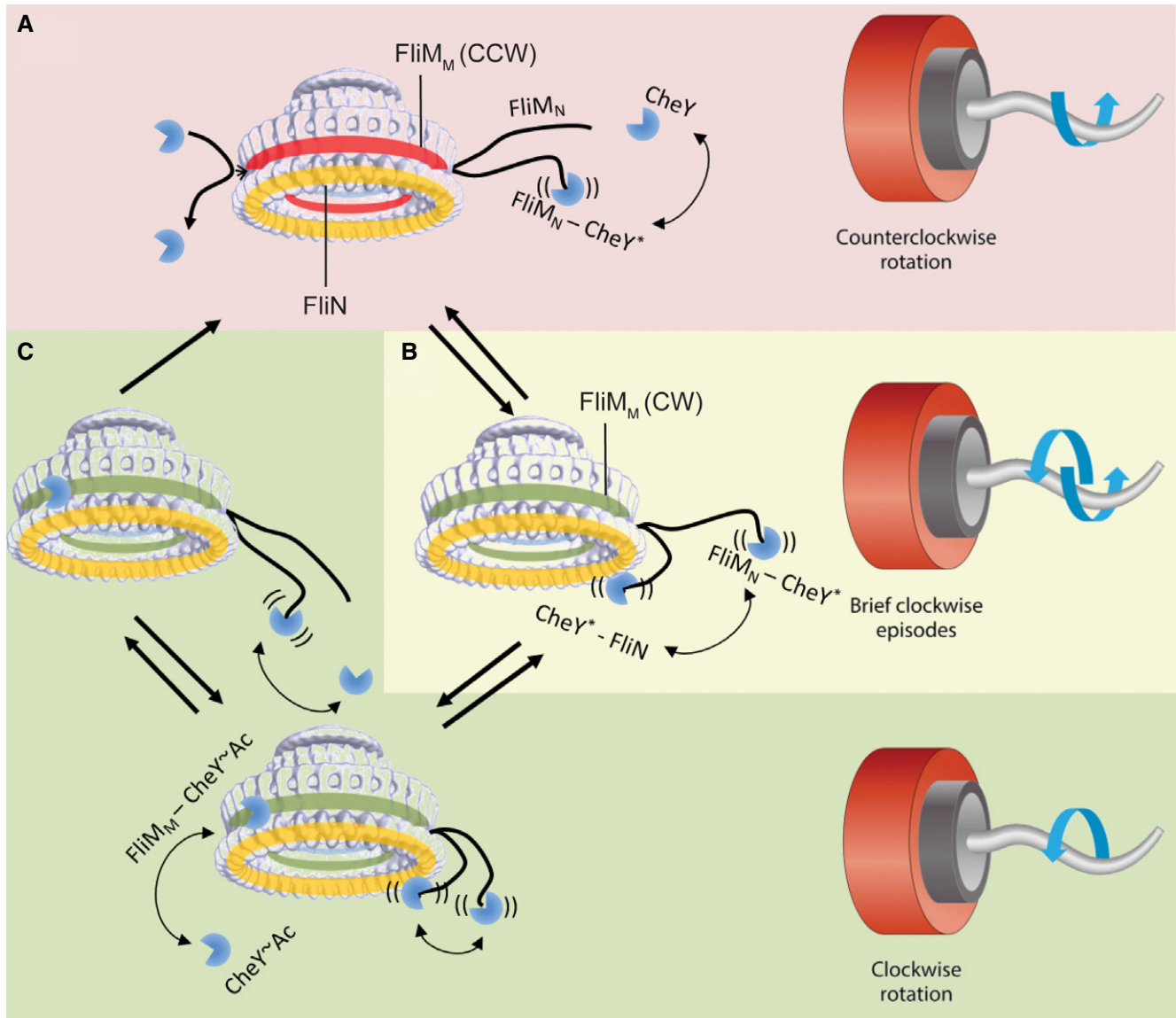


Figure 6. A model for clockwise generation by CheY-P and CheY-Ac.

The model suggests the most likely interactions of CheY at the switch. Yellow ring, FliN. Green or red ring, FliM_M in a conformation to which CheY can or cannot bind, respectively. Red background region is counterclockwise rotation. Yellow background region is frequent switching. Green-shaded region is clockwise rotation.

- A** When the motor rotates counterclockwise, CheY most likely binds to FliM_N because FliM_N is a high-affinity site and because it is the most accessible site. An interaction of CheY with FliN is not probable at physiological CheY concentrations, unless CheY first binds to FliM_N. Binding to FliM_N potentiates CheY, making it more likely to act on FliN. (Potentiated CheY is marked with an asterisk) FliM_M is probably sterically blocked for CheY binding or is in a conformation that does not favor CheY binding.
- B** FliM_N-bound CheY has high probability of interacting with FliN. This interaction generates brief episodes of clockwise rotation, because the complex CheY-FliN is unstable and is likely to quickly dissociate.
- C** During the short episodes of clockwise rotation shown in B, FliM_M either becomes accessible to CheY or is changed to a conformation that favors CheY binding. As a result, CheY (or, most likely, CheY-Ac) binds to FliM_M. This binding stabilizes the clockwise conformation of FliM_M and prevents the latter from resuming its counterclockwise conformation or becoming again sterically blocked for CheY binding. As long as CheY is bound to FliM_M, CheY dissociation from FliN no longer affects clockwise rotation. CheY dissociation from FliM_M when CheY is already dissociated from FliN would cause an immediate return to counterclockwise rotation. See text for other details.

of clockwise generation (Fig 6A), which may have evolved to filter out crosstalk with proteins having CheY-like folds in other two-component signaling pathways. (Binding of such proteins to FliM_N is expected to be futile.)

The meaning of CheY potentiation in molecular terms is not known. According to the view that confined segments of CheY switch asynchronously and locally between active and inactive conformations (McDonald *et al*, 2012), perhaps CheY binding to

FliM_N stabilizes a distinct conformation that is most potent for clockwise generation. Since FliM_N-bound CheY is more rapidly phosphorylated by small phosphodonors (Schuster *et al*, 2001), it is reasonable that in this clockwise-promoting conformation, the phosphorylation site is more accessible to small phosphodonors. To test the possibility that CheY binding to FliM_N indeed stabilizes a distinct conformation that is most potent for clockwise generation, it might be of interest to simulate or solve the conformation of an extremely potent CheY variant, such as FliM_N-CheY(D13K), and thereby derive the form of CheY that preforms the switching action at the motor.

Remarkably, the ultrasensitivity of the switch, observed in FliM_{wt} motors as a sigmoidal (cooperative) clockwise dependence on the intracellular CheY~P level (Cluzel *et al*, 2000), is lost in FliM_{ΔN} motors (Fig 2G). This suggests that FliM_N has a role here too. (Note, though, that CheY~Ac, which appears to bind to the switch more firmly than does CheY~P, exhibits sigmoidal dependence—Fig 2G; see below) The published finding that a constitutively active CheY mutant protein binds better to clockwise-rotating motors than to counterclockwise-rotating motors (Fukuoka *et al*, 2014) and the notion that this can generate cooperative binding (Duke *et al*, 2001), combined with the possibility, raised above, that CheY binding to FliM_N may stabilize a distinct conformation that is most potent for clockwise generation, may explain why switch ultrasensitivity requires FliM_N.

The switching mechanism: an apparent gating mechanism

This study suggests that CheY~P binds to FliN with resultant transient switches of the motor to clockwise rotation and that CheY~Ac preferentially binds to FliM_M to produce stable clockwise rotation. [Note that an *E. coli* cell always contains some level of CheY~Ac, even in the absence of acetate (Yan *et al*, 2008; Fraiberg *et al*, 2015).] These are based on (i) the conclusions, made above, that short intervals are mostly promoted by CheY binding to FliN, and long intervals—by CheY binding to FliM_M, (ii) the observation that the dwell time of CheY~P at the motor (Fig 1F) is shorter than that of CheY~Ac (Fig 1E), and (iii) the finding that CheY~Ac is more effective than CheY~P in clockwise generation (Fig 2G). We propose that, following CheY~P potentiation by FliM_N, CheY~P mainly binds to FliN to make the first catalytic step of clockwise generation, producing brief episodes of clockwise rotation (Fig 6B), and that CheY~Ac mainly binds to FliM_M and makes the second catalytic step of clockwise generation, stabilizing the rotation in the clockwise direction (Fig 6C). It is probable that CheY~P and CheY~Ac can also bind to FliM_M and FliN, respectively, though at much lesser affinity. We assume that CheY, activated by phosphorylation or acetylation, can bind to FliN at any time, but it can only bind to FliM_M when the motor already rotates clockwise to some extent. This assumption relies on the observation that the orientation of a FliM subunit within the switch is different in the counterclockwise and clockwise states (Paul *et al*, 2011), which may cause FliM_M to be sterically blocked for CheY binding in the counterclockwise conformation. Thus, clockwise rotation, which results from CheY binding to FliN, exposes the CheY-binding site at FliM_M. We term such a mechanism, which involves a conditional binding, a “gating mechanism”. This mechanism is consistent with the kinetic model (Appendix Fig S5), proposed to explain the sequential appearance of two phases in

the response of FliM_{ΔN} motors to acetate removal (Fig 3B). This kinetic model appears to be conceptually similar to the model of conformational spread (Duke *et al*, 2001; Bai *et al*, 2010).

The gating mechanism may provide an explanation of the different dependences of clockwise generation on the levels of CheY~P and CheY~Ac—saturation and sigmoidal curves, respectively (Fig 2G). Binding of CheY~P, according to this study, is mainly to FliN. The binding site at FliN is accessible to CheY~P, for which reason the dependence of clockwise generation (which reflects CheY~P binding to the switch) on the intracellular level of CheY~P would have the shape of a saturation curve. In contrast, CheY~Ac preferentially binds to FliM_M, whose accessibility is, as explained above, conditional. The availability of more and more binding sites at FliM_M as the level of intracellular CheY increases is likely to generate a sigmoidal, cooperative-like dependence.

The gating mechanism may also support efficient swimming. As mentioned in the introduction, when some of the motors in a given bacterial cell exhibit extremely brief episodes of clockwise rotation, the swimming direction is maintained at large, and the outcome is directionally persistent migration of the cell population (Vladimirov *et al*, 2010; Saragosti *et al*, 2011). Such directional persistence may markedly improve collective migration (Saragosti *et al*, 2011). On the other hand, tumbling behavior, which reorients the swimming direction to support the classical run-and-tumble view of bacterial migration (Berg, 2003; Eisenbach, 2004), requires relatively long clockwise rotation intervals. The gating mechanism can generate both types of swimming behavior because it can produce both short and long clockwise intervals. Indeed, a small-scale study, performed by us, suggested that the short intervals of clockwise rotation needed for directional persistence (Saragosti *et al*, 2011) could, indeed, be provided by CheY~P binding to FliN and that the long clockwise intervals for tumbling could be provided by CheY~Ac binding to FliM_M (Appendix 2 and Appendix Fig S9). This means that the switching mechanism is wired to inputs from two different signaling pathways: One involves the chemotaxis machinery that regulates CheY phosphorylation, and the other involves the cellular metabolic pathway that regulates CheY acetylation. Hence, this switching mechanism apparently optimizes chemotactic performance according to the ambient conditions.

Unique features of the switching mechanism

The switching mechanism, revealed in this study, has a number of unique features. On the one hand, it is tightly regulated by three distinct binding sites and by two different covalent modifications. Binding to the second site, FliN, depends on phosphorylation of CheY, and binding to the third site, FliM_M, mainly depends on acetylation. This binding can apparently occur only if it is preceded by CheY~P binding to FliN. On the other hand, this mechanism endows the motor with flexibility with respect to switching, as the intermediate stage at which CheY~P is bound to FliN provides a “go/no go” situation, in which the motor can either proceed to a stable clockwise rotation due to binding to FliM_M or shift back to counterclockwise rotation. With this unique combination of seemingly conflicting, but complementing properties of the switching mechanism, it would not be surprising if similar mechanisms are found in the future in the output of other signaling systems.

Materials and Methods

Strains and plasmids

Strains and plasmids used in this study are listed in Appendix Tables S1 and S2, respectively. To produce *fliM_N* truncation, *fliM-YPet* was cloned from the strain JPA945 (Delalez *et al.*, 2010) (kindly provided by J. Armitage) with genomic flanks of 500 base pairs to the Pst1 sites of pDS132 suicide plasmid (Philippe *et al.*, 2004). FliM residues 1–16 were truncated from the resulting plasmid by RF cloning. The constructed plasmid was used to perform allelic exchange with strain JPA945 to produce strain EW566 bearing *fliMΔ(1–16)-YPet* genomic mutation. The mutation was verified by PCR sequencing. Plasmidic mutations were produced by RF cloning. The genomic deletion mutations of *cheA* and *cheZ* were produced by subjecting cells to P1 transduction with phage containing the genetic background of strain JW1870 or JW1877, respectively.

Growth conditions

Strains, diluted 1:100 from overnight cultures, were cultured to mid-late exponential phase at 30°C in tryptone broth with appropriate antibiotics to maintain the plasmids. For CheY expression, cells were grown to mid-late exponential phase and induced by IPTG for 3–4 h. It appeared that overnight cultures which, prior to being diluted, had been left on the bench at room temperature for 1–2 days, gave rise to cultures that produced better responses to acetate.

Analysis of the direction of flagellar rotation

The direction of flagellar rotation was determined by the tethering assay (Silverman & Simon, 1974). Subsequent to flagellar partial truncation by passing the bacterial culture in a syringe several times, the resulting suspension was usually washed three times in motility buffer (10 mM KP_i pH 7.0, 0.1 mM EDTA). The cells were tethered to a coverslip in a flow chamber as described (Berg & Block, 1984) and washed with motility buffer in the flow chamber for roughly 5 min prior to measurement. All chemicals used in behavioral assays were dissolved in the motility buffer. Documentation was done with a uEye digital camera on top of a Zeiss phase-contrast microscope. Recording was typically done at 75 frames/s. The time of reagents' entry to the flow chamber (~20 s from the time of introducing the reagent to the pump's pipe) was estimated by the chemotactic response of wild-type cells. The time needed for replacement of the total chamber's volume was 6 s.

Automated analysis of flagellar motor direction of rotation

All the analyses were done with a pack of MATLAB scripts prepared for this study. These are freely available at <https://github.com/OshriAfanzar/Afanzar-et-al-2019>. All samples of all experiments were analyzed in the exact same way and codes.

Frame and movie processing

Each frame was processed by the following scheme: Image binarization → Identification of connected pixels → Ellipse fitting to bodies

of connected pixels. Image binarization process was written in MATLAB as the following code lines:

```
Pixels = vidFrame(:);
SortedPixels = sort(Pixels);
LinearBase = linspace(min(Pixels),max(Pixels),
length(Pixels));
SubtractPixels = SortedPixels - LinearBase;
Tresh = mean(SortedPixels (find(SubtractPixels,min
(SubtractPixels))));
vidFrame = (vidFrame - Tresh)>0;
```

Connected pixels were extracted by the “bwconncomp” function of MATLAB and ellipse fitting was done using the “regionprops” function of MATLAB. Trajectories of rotating cells were composed by identifying ellipses that shared common pixels area for at least 95% of the recording time. The value of 95% was chosen because during the recording there were sometimes events of missing acquisitions (e.g., out of focus events) and we reasoned that we can trust a cell recording only when it could be identified for at least 95% of the recording time. Trajectories in which the rotation was not smooth (e.g., in cases where the rotation frequently paused, or where the rotation was not in a 2D plain) and, therefore, contained over-represented rotation angles, were spotted and discarded. The way to spot over-represented angles was to calculate the extent by which the distribution of angles deviates from random distribution. Thus, we found empirically that when we employed bins of 10° for calculating the distribution of angles, trajectories that contained one or more bins with a number of counts exceeding the number [(total number of counts)*2/(number of bins)] were suspicious and discarded.

Analysis of rotation

Angles extracted from the fitted ellipses were used to calculate rotation velocity as the difference in cell angle with respect to the frame rate. To ensure high-quality data, events in which the fitted ellipse met the following stringent conditions were marked as erroneous: (i) Major axis/Minor Axis < 1.25. (ii) Major axis < 7 pixels. (iii) Major axis < mean(Major axis) – 2SD(Major axis). (iv) Major axis > mean(Major axis) + 2SD(Major axis). (v) Angular displacement was < 360°/frame rate (e.g., 360/75 for 75 frames/s) or > 10*360°/frame rate (e.g., 3600/75 for acquisition frequency of 75 frames/s). When a single erroneous event was flanked by intervals of a different type, the erroneous event was replaced by an event whose identity was determined by the calculated rate of rotation. For example, for clockwise = →, counterclockwise = ← and erroneous interval = E, for the sequence ←←←←E→→→→, which corresponds to the rotation rates (–5)(–5)(–5)(–5)(0.4)(5)(5)(5)(5) Hz, E would be replaced by → because the erroneous interval 0.4 is positive, i.e., with clockwise tendency.

Calculation of the fraction of time spent in clockwise rotation

The fraction of time that a motor spent in clockwise rotation was calculated as the sum of clockwise events in a unit time. For steady state rotation, the fraction of time spent in clockwise rotation was calculated for the whole time of acquisition (typically, 30 s) and averaged over all cells. For time-resolved rotation (as in the response to stimuli), clockwise rotation of single cells was averaged in 1-s intervals.

Analysis of interval length

We defined clockwise intervals as intervals that have at least four consecutive frames of clockwise rotation at a rate higher than 1 Hz. The rotation rate value was taken as two standard deviations away from the rotation rate control of non-rotating cells [the rotation rate of these cells was 0 ± 0.5 Hz (\pm SD)]. This 4-frame threshold excluded short events that might not be CheY-mediated clockwise rotation. The choice of four frames (52 ms) for the threshold was according to another negative control, consisting of a Δ *CheY* strain, which cannot generate CheY-mediated clockwise rotation. In this negative-control strain, we studied 1-min recordings of 344 cells, and found ~100 clockwise intervals, all shorter than 50 ms. To avoid artifacts that might have been caused by interactions between the cell body and the surface, we also excluded from the analysis intervals that were flanked by pause events. All excluded intervals were considered erroneous. We grouped clockwise intervals from cells that had similar average clockwise levels and produced from each group a distribution of interval lengths. Intervals were measured only when they were flanked by intervals of the opposite direction, and were not flanked by erroneous intervals. For example, for clockwise = \rightarrow , counterclockwise = \leftarrow , and erroneous interval = E, the sequence of intervals $\leftarrow\leftarrow\leftarrow\leftarrow\rightarrow\rightarrow\rightarrow\rightarrow\leftarrow\leftarrow\leftarrow\leftarrow$ would resolve in only one interval of clockwise rotation at the length of four frames. When a single erroneous event was flanked by intervals of the same type, the erroneous event was replaced by an event of the same type as the flanks. For example, $\leftarrow\leftarrow\leftarrow\leftarrow\leftarrow\leftarrow$ would be replaced by $\leftarrow\leftarrow\leftarrow\leftarrow\leftarrow\leftarrow$.

Analysis of reversal frequency

The reversal frequency was defined as the number of zero-velocity crossing events per second (after filtering for noise).

In vivo FRET response to stimuli

FRET measurements in response to stimuli were carried out as described by Sourjik and Berg (2002).

Measurements of CheY expression levels

To assess CheY levels in the cytoplasm, cells expressing CheY-mCherry or mCherry from a plasmid (strains EW575 and EW569, respectively) were grown to mid-late exponential phase and induced by various IPTG concentrations for 4 or 6 h. The cells were washed three times in NaPi (10 mM, pH 7.6). A sample of the cells was plated in serial dilutions on LB-agar plates to estimate, by colony forming units, the number of cells in the culture. The rest of the sample was sonicated and loaded in 200 μ l aliquots to a 96-well plate. In the same plate, a purified CheY-mCherry protein at a known concentration was loaded in different dilutions. The plate was read by a Cytation-5 plate reader (excitation and emission filters were 570 ± 20 nm and 610 ± 20 nm, respectively). The calculation of the cellular concentration of the expressed proteins assumed that the average volume of a single cell is 1 fl.

Single-molecule observation and analysis

The protein 6xHis-CheY(I95V) was purified by Protino Ni-TED beads and labeled with a maleimide modification of the organic dye

Atto647, previously shown to be bright, photo-stable, not hydrophobic and, therefore, highly compatible with observation of single molecules *in vivo* (Plochowitz et al, 2014). The labeled protein was separated from the residual unreacted dye by size-exclusion chromatography and was then electroporated into cells of strain EW669 in a low-salinity buffer. The electroporation approach was carried out as described (Di Paolo et al, 2016). The electroporated cells were recovered for 5 min in Super Optimal broth with Catabolite repression, washed 4–5 times in motility buffer, and visualized on agar pads on a customized inverted Olympus IX-71 microscope equipped with two lasers, a 637 nm diode laser (Vortran Stradus; Vortran Laser Technology, Sacramento, CA, USA) and a 532 nm DPSS laser (MGL-III-532 nm-100 mW, CNI) (Appendix Fig S10A). Laser light was combined into a single-mode optical fiber (Thorlabs, Newton, NJ, USA) and collimated before focusing on the objective. Highly inclined and laminated optical sheet (HILO) and total internal reflection fluorescence illuminations were achieved by adjusting the position of the focused excitation light on the back focal plane of the objective (UPLSAPO, 100 \times , NA 1.4, Olympus). Cellular fluorescence was collected through the same objective, filtered to remove excitation light through a long-pass filter (HQ545LP; Chroma, Taoyuan Hsien, Taiwan) and a notch filter (NF02-633S; Semrock, Rochester, NY, USA), and spectrally separated by a dichroic mirror (630DRLP, Omega, Brattleboro, VT, USA). Each channel was imaged onto separate halves of the chip of an EMCCD camera (iXon+, BI-887, Andor, Belfast, UK). The illumination for bright-field images comprised a white-light lamp (IX2-ILL100; Olympus, Shinjuku, Tokyo, Japan) and condenser (IX2-LWUCD; Olympus) attached to the microscope. Movies and images were recorded at 100 frames/s using manufacturer's software (Andor). All measurements were carried out in continuous wave mode for both green and red lasers. For all the experiments, the exposure time was 10 ms and the intensities used for YPet and Atto647 were 400 nW μ m⁻² and 1 μ W μ m⁻², respectively.

The locations of CheY(I95V)-Atto647 and FliM-YPet were automatically estimated by a custom-made MATLAB script. Switch locations were identified as peaks of fluorescence. The exact switch location was determined by identifying the location of the maximum of a 2D Gaussian, fitted to each switch spot. For the identification of switches, several images were acquired, normalized, and averaged before Atto647 imaging. The location of CheY(I95V)-Atto647 was determined similarly to switch location in each frame. CheY(I95V)-Atto647 was considered bound to the switch when it was within 75 nm of a switch location for at least 30 ms. The choice of 75 nm was based on the motor radius (25 nm) combined with the expected length of FliM_N (assuming 15 nm FliM_N length, considering about 3.5 Å per amino acid residue). The distance of 75 nm is more permissive than the expected binding radius (40 nm) because we expected some inaccuracy in the localization of the motor. Dwell times < 30 ms were excluded to avoid false-positive measurements (e.g., molecules diffusing near the motor). The value of 30 ms (three frames) was chosen as the half of the expected mean dwell time of CheY(I95V)-Atto647 with FliM_N [~60 ms given a $K_d = 3.9$ μ M for CheY(I95V)-FliM_N interaction (Schuster et al, 2000) and an estimated $k_{on} = 4 \times 10^6$ M⁻¹ s⁻¹ (Sourjik & Berg, 2002)]. The mean-square displacement in two dimensions due to free diffusion is $\langle r^2 \rangle = 4Dt$. Setting $\langle r^2 \rangle = 75$ nm² and $t = 30$ ms yields $D = 0.047$ μ m² s⁻¹, which is much lower than the diffusion coefficient

of CheY in the cell [estimated to be 50–100 $\mu\text{m}^2 \text{s}^{-1}$ (Segall *et al.*, 1985)]. Thus, a false-positive rate due to diffusing CheY molecules is expected to be negligible. Trajectories from the same type of experiments were joined for survival analysis (Fig S10B). The number of cells recorded was 82 (ΔcheZ no acetate), 40 (ΔcheZ with acetate), 63 (ΔcheA no acetate), and 56 (ΔcheA with acetate). The number of trajectories in which CheY was found to interact with FliM was 2414 (ΔcheZ no acetate), 2660 (ΔcheZ with acetate), 1316 (ΔcheA no acetate), and 1904 (ΔcheA with acetate).

Data availability

All the source data from this publication have been deposited to the Biostudies database <https://www.ebi.ac.uk/biostudies/> and assigned the identifier S-BSST558.

Expanded View for this article is available online.

Acknowledgements

We are indebted to Dr. David Blair and Paige Wheatley in his group for numerous intensive discussions, for critical reading of earlier versions of the manuscript, for disclosing their unpublished data, and for providing some of the mutants used in this study. We thank Dr. James E. Ferrell for his advice in the construction of the mathematical model, Dr. Ady Vaknin and Vered Frank in his group for allowing us to measure FRET in their laboratory and for their useful suggestions and technical assistance, Dr. S. Roy Caplan for helpful discussions, Vladimir Kiss for assistance with operating the confocal microscope, Dr. Judith Armitage for supplying bacterial strains, and Yana Gurevich for technical assistance. This study was supported by grant no. 2013197 from the US-Israel Binational Science Foundation and by grant no. 66/14 from the Israel Science Foundation to ME, by a UK BBSRC grant no. BB/H01795X/1 and an ERC Starter grant no. ERC 261227 to ANK, and by a BBSRC grant to RMB. DDP was supported by a UK EPSRC DTC studentship. AP was supported by a UK EPSRC DTA studentship and the German National Academic Foundation (Studienstiftung) and the Phizackerley Senior Scholarship in Medical Sciences at Balliol College, Oxford. OA was supported by an EMBO short term travel fellowship to Oxford.

Author contributions

Performing and analyzing the experiments: OA; Designing the experiments, result interpretation, and manuscript writing: OA, MEisenbach; Docking analysis: OA, MEisenstein; Some of the experiments and technical assistance: KL; Single-molecule electroporation experiment analysis: DDP, OA; TIRF setup: ANK; Insight interpreting the single-molecule results and providing important input for the data analysis of the tethering experiments and for writing the manuscript: RMB; Sharing a script that helped with image alignment: AP.

Conflict of interest

The authors declare that they have no conflict of interest.

References

Bai F, Branch RW, Nicolau DV, Pilizota T, Steel BC, Maini PK, Berry RM (2010) Conformational spread as a mechanism for cooperativity in the bacterial flagellar switch. *Science* 327: 685–689

- Barak R, Welch M, Yanovsky A, Oosawa K, Eisenbach M (1992) Acetyladenylate or its derivative acetylates the chemotaxis protein CheY *in vitro* and increases its activity at the flagellar switch. *Biochemistry* 31: 10099–10107
- Barak R, Abouhamad WN, Eisenbach M (1998) Both acetate kinase and acetyl Coenzyme A synthetase are involved in acetate-stimulated change in the direction of flagellar rotation in *Escherichia coli*. *J. Bacteriol.* 180: 985–988
- Barak R, Eisenbach M (1999) Chemotactic-like response of *Escherichia coli* cells lacking the known chemotaxis machinery but containing overexpressed CheY. *Mol Microbiol* 31: 1125–1137
- Barak R, Eisenbach M (2001) Acetylation of the response regulator, CheY, is involved in bacterial chemotaxis. *Mol Microbiol* 40: 731–743
- Barak R, Eisenbach M (2004) Co-regulation of acetylation and phosphorylation of CheY, a response regulator in chemotaxis of *Escherichia coli*. *J Mol Biol* 342: 375–381
- Barak R, Prasad K, Shainskaya A, Wolfe AJ, Eisenbach M (2004) Acetylation of the chemotaxis response regulator CheY by acetyl-CoA synthetase from *Escherichia coli*. *J Mol Biol* 342: 383–401
- Berg HC, Brown DA (1972) Chemotaxis in *Escherichia coli* analysed by three-dimensional tracking. *Nature* 239: 500–504
- Berg HC, Block SM (1984) A miniature flow cell designed for rapid exchange of media under high-power microscope objectives. *J Gen Microbiol* 130: 2915–2920
- Berg HC (2003) The rotary motor of bacterial flagella. *Annu Rev Biochem* 72: 19–54
- Borkovich KA, Kaplan N, Hess JF, Simon MI (1989) Transmembrane signal transduction in bacterial chemotaxis involves ligand-dependent activation of phosphate group transfer. *Proc Natl Acad Sci USA* 86: 1208–1212
- Bourret RB, Hess JF, Simon MI (1990) Conserved aspartate residues and phosphorylation in signal transduction by the chemotaxis protein CheY. *Proc Natl Acad Sci USA* 87: 41–45
- Bren A, Eisenbach M (1998) The N terminus of the flagellar switch protein, FliM, is the binding domain for the chemotactic response regulator, CheY. *J Mol Biol* 278: 507–514
- Cluzel P, Surette M, Leibler S (2000) An ultrasensitive bacterial motor revealed by monitoring signaling proteins in single cells. *Science* 287: 1652–1655
- Cross FR, Archambault V, Miller M, Klovstad M (2002) Testing a mathematical model of the yeast cell cycle. *Mol Biol Cell* 13: 52–70
- Delalez NJ, Wadhams GH, Rosser G, Xue Q, Brown MT, Dobbie IM, Berry RM, Leake MC, Armitage JP (2010) Signal-dependent turnover of the bacterial flagellar switch protein FliM. *Proc Natl Acad Sci USA* 107: 11347–11351
- Di Paolo D, Afanзар O, Armitage JP, Berry RM (2016) Single-molecule imaging of electroporated dye-labelled CheY in live *Escherichia coli*. *Philos Trans R Soc Lond B Biol Sci* 371: 20150492
- Duke TAJ, Le Novère N, Bray D (2001) Conformational spread in a ring of proteins: a stochastic approach to allostery. *J Mol Biol.* 308: 541–553
- Dyer CM, Dahlquist FW (2006) Switched or not?: the structure of unphosphorylated CheY bound to the N terminus of FliM. *J Bacteriol* 188: 7354–7363
- Dyer CM, Vartanian AS, Zhou H, Dahlquist FW (2009) A molecular mechanism of bacterial flagellar motor switching. *J Mol Biol* 388: 71–84
- Eisenbach M, Caplan SR (1998) Bacterial chemotaxis: unsolved mystery of the flagellar switch. *Curr Biol* 8: R444–R446
- Eisenbach M (2004) Bacterial chemotaxis. In *Chemotaxis*, Eisenbach M (ed.), pp 53–215, London: Imperial College Press
- Fraiberg M, Afanзар O, Cassidy CK, Gabashvili A, Schulten K, Levin Y, Eisenbach M (2015) CheY's acetylation sites responsible for generating clockwise flagellar rotation in *Escherichia coli*. *Mol Microbiol* 95: 231–244

- Fukuoka H, Sagawa T, Inoue Y, Takahashi H, Ishijima A (2014) Direct imaging of intracellular signaling components that regulate bacterial chemotaxis. *Sci Signal* 7: ra32
- Kihara M, Macnab RM (1981) Cytoplasmic pH mediates pH taxis and weak-acid repellent taxis of bacteria. *J Bacteriol* 145: 1209–1221
- Laslo P, Spooner CJ, Warmflash A, Lancki DW, Lee H-J, Sciammas R, Gantner BN, Dinner AR, Singh H (2006) Multilineage transcriptional priming and determination of alternate hematopoietic cell fates. *Cell* 126: 755–766
- Li M, Hazelbauer GL (2004) Cellular stoichiometry of the components of the chemotaxis signaling complex. *J Bacteriol* 186: 3687–3694
- Li R, Gu J, Chen YY, Xiao CL, Wang LW, Zhang ZP, Bi LJ, Wei HP, Wang XD, Deng JY et al (2010) CobB regulates *Escherichia coli* chemotaxis by deacetylating the response regulator CheY. *Mol Microbiol* 76: 1162–1174
- Liarzi O, Barak R, Bronner V, Dines M, Sagi Y, Shainskaya A, Eisenbach M (2010) Acetylation represses the binding of CheY to its target proteins. *Mol Microbiol* 76: 932–943
- Mathews MAA, Tang HL, Blair DF (1998) Domain analysis of the FlIM protein of *Escherichia coli*. *J Bacteriol* 180: 5580–5590
- McDonald LR, Boyer JA, Lee AL (2012) Segmental motions, not a two-state concerted switch, underlie allostery in CheY. *Structure* 20: 1363–1373
- McEvoy M, Bren A, Eisenbach M, Dahlquist FW (1999) Identification of the binding interfaces on CheY for two of its targets, the phosphatase CheZ and the flagellar switch protein FlIM. *J Mol Biol* 289: 1423–1433
- Paul K, Brunstetter D, Titen S, Blair DF (2011) A molecular mechanism of direction switching in the flagellar motor of *Escherichia coli*. *Proc Natl Acad Sci USA* 108: 17171–17176
- Philippe N, Alcaraz J-P, Coursange E, Geiselmann J, Schneider D (2004) Improvement of pCVD442, a suicide plasmid for gene allele exchange in bacteria. *Plasmid* 51: 246–255
- Plochowitz A, Crawford R, Kapanidis AN (2014) Characterization of organic fluorophores for in vivo FRET studies based on electroporated molecules. *Phys Chem Chem Phys* 16: 12688–12694
- Pomerening JR (2008) Uncovering mechanisms of bistability in biological systems. *Curr Opin Biotechnol* 19: 381–388
- Porter SL, Wadhams GH, Armitage JP (2011) Signal processing in complex chemotaxis pathways. *Nat Rev* 9: 153–165
- Repaske DR, Adler J (1981) Change in intracellular pH of *Escherichia coli* mediates the chemotactic response to certain attractants and repellents. *J Bacteriol* 145: 1196–1208
- Sagi Y, Khan S, Eisenbach M (2003) Binding of the chemotaxis response regulator CheY to the isolated, intact switch complex of the bacterial flagellar motor: lack of cooperativity. *J Biol Chem* 278: 25867–25871
- Saragosti J, Calvez V, Bournaveas N, Perthame B, Buguin A, Silberzan P (2011) Directional persistence of chemotactic bacteria in a traveling concentration wave. *Proc Natl Acad Sci USA* 108: 16235–16240
- Sarkar MK, Paul K, Blair D (2010) Chemotaxis signaling protein CheY binds to the rotor protein FlIN to control the direction of flagellar rotation in *Escherichia coli*. *Proc Natl Acad Sci USA* 107: 9370–9375
- Scharf BE, Fahrner KA, Turner L, Berg HC (1998) Control of direction of flagellar rotation in bacterial chemotaxis. *Proc Natl Acad Sci USA* 95: 201–206
- Schuster M, Zhao R, Bourret RB, Collins EJ (2000) Correlated switch binding and signaling in bacterial chemotaxis. *J Biol Chem* 275: 19752–19758
- Schuster M, Silversmith RE, Bourret RB (2001) Conformational coupling in the chemotaxis response regulator CheY. *Proc Natl Acad Sci USA* 98: 6003–6008
- Segall JE, Ishihara A, Berg HC (1985) Chemotactic signaling in filamentous cells of *Escherichia coli*. *J Bacteriol* 161: 51–59
- Silverman M, Simon M (1974) Flagellar rotation and the mechanism of bacterial motility. *Nature* 249: 73–74
- Sourjik V, Berg HC (2002) Binding of the *Escherichia coli* response regulator CheY to its target measured *in vivo* by fluorescence resonance energy transfer. *Proc Natl Acad Sci USA* 99: 12669–12674
- Terashima H, Kojima S, Homma M (2008) Flagellar motility in bacteria structure and function of flagellar motor. *Int Rev Cell Mol Biol* 270: 39–85
- Thomas DR, Francis NR, Xu C, DeRosier DJ (2006) The three-dimensional structure of the flagellar rotor from a clockwise-locked mutant of *Salmonella enterica serovar Typhimurium*. *J Bacteriol* 188: 7039–7048
- Turner L, Ryu WS, Berg HC (2000) Real-time imaging of fluorescent flagellar filaments. *J Bacteriol* 182: 2793–2801
- Vladimirov N, Lebedez D, Sourjik V (2010) Predicted auxiliary navigation mechanism of peritrichously flagellated chemotactic bacteria. *PLoS Comput Biol* 6: e1000717
- Welch M, Oosawa K, Aizawa SI, Eisenbach M (1993) Phosphorylation-dependent binding of a signal molecule to the flagellar switch of bacteria. *Proc Natl Acad Sci USA* 90: 8787–8791
- Wolfe AJ, Conley MP, Berg HC (1988) Acetyladenylate plays a role in controlling the direction of flagellar rotation. *Proc Natl Acad Sci USA* 85: 6711–6715
- Yan J, Barak R, Liarzi O, Shainskaya A, Eisenbach M (2008) *In vivo* acetylation of CheY, a response regulator in chemotaxis of *Escherichia coli*. *J Mol Biol* 376: 1260–1271



License: This is an open access article under the terms of the Creative Commons Attribution-NonCommercial-NoDerivs License, which permits use and distribution in any medium, provided the original work is properly cited, the use is non-commercial and no modifications or adaptations are made.